

ELASTIC ELECTRON-DEUTERON SCATTERING AT HIGH ENERGY*

Raymond G. Arnold
The American University
Washington, DC 20016

and

Stanford Linear Accelerator Center
Stanford University, Stanford, California 94305

and

Carl E. Carlson and Franz Gross
Department of Physics
College of William and Mary, Williamsburg, VA 23185

Submitted to Physical Review C

* Work supported by the Department of Energy under contract number
DE-AC03-76SF00515.

ABSTRACT

Relativistic formulae for the deuteron electromagnetic form factors are calculated in the impulse approximation retaining terms to all orders in $Q^2/M^2 \approx (v/c)^2$. The formulae are given as double integrals over the deuteron wave functions in momentum space, and hence can be evaluated for any deuteron model. We evaluate these formulae numerically for 9 different deuteron models: Reid soft core, two Lomon-Feshbach models, three Holinde-Machleidt models, and three four-component relativistic models. All of the models give results for the A structure function considerably below the experimental results; the effect of the relativistic treatment is to reduce the size of A by a factor of 2 to 5 at Q^2 of 100 fm^{-2} over what it would be in the nonrelativistic approximation. We discuss briefly the role of exchange currents; the pair terms are included in our calculation in a completely consistent manner, but the explicit $\rho\pi\gamma$ contributions need to be calculated relativistically. We discuss in some detail the sensitivity of our calculation to the almost unknown neutron electric form factor, observing that a G_{En} roughly twice G_{Ep} in the region of $Q^2 = 100 \text{ fm}^{-2}$ would enable us to fit the data even without any $\rho\pi\gamma$ contributions. We discuss the high Q^2 limits of our formulae, obtaining the result that the form factor falls one power of Q^2 faster than that predicted by the dimensional scaling quark model. We also study the low Q^2 limits and give explicit formulae for the corrections to the deuteron magnetic and quadrupole moments.

I. Introduction and Summary

Recent measurements¹ have made it necessary to calculate electron deuteron elastic scattering without making nonrelativistic approximations or q^2/M^2 expansions. Here we report in some detail on a relativistic calculation of the deuteron electromagnetic form factors in the impulse approximation (RIA), retaining terms to all orders in q^2/M^2 . A short description of our results has been published previously.²

There are two effects that one must take into account in a relativistic calculation, and we have done both.

(i) The kinematics must be relativistic. Our calculation is covariant, and our final formulae contain kinematic effects to all orders in $(v/c)^2$ or q^2/M^2 .

(ii) At least one of the nucleons must be off the mass shell. We include the most important consequences of this by allowing the interacting nucleon to be off shell, while still leaving the spectator on shell. In this way, the covariant diagram of Fig. 1(a) includes the three-time ordered diagrams of Fig. 1(b), and important effects such as the photon splitting into an $\bar{N}N$ pair (the "pair current" in other language) are properly included. However, in order to do this, we must also know about amplitudes for $\bar{N} + d \rightarrow N$, as well as the usual $d \rightarrow NN$. This is best handled in a unified way by considering a covariant deuteron-nucleon-nucleon vertex function, with one nucleon off shell.

Following Blankenbecler and Cook,³ four invariants must be used to describe the deuteron-nucleon-nucleon vertex function. (In a nonrelativistic treatment, one makes an approximation by putting both nucleons on shell so that only two invariants are needed.) The four scalar functions

that are necessary can be rewritten so that they have the character of wavefunctions.⁴ When this is done, two of the functions are the familiar S and D state wavefunctions of the deuteron, and there are two additional wavefunctions which are not present in the nonrelativistic case. These new components of the full wavefunction are associated with the extra degrees of freedom present when the interacting nucleon is a virtual Dirac particle, and each has the character of a P-state. They are numerically small if measured by their contribution to the overall normalization of the wavefunction, but in momentum space they and the S and D wavefunctions have comparable magnitudes at high momenta. (We should note that although the orbital angular momentum of these small components is $l = 1$, they do not represent parity violating effects because, in common with the small components in the Dirac equation, the overall parity of a small component is opposite to its spatial parity.)

The formulae that we derive are general and may be evaluated with any deuteron wavefunctions. In particular, if one chooses to neglect the P-states, the calculation gives the deuteron form factor correctly to all orders of $(q/M)^2$ for any choice of u and w , the S and D-state wavefunctions.

In addition to deriving the formulae, we have evaluated them numerically for a number of deuteron wavefunctions and have examined them analytically to determine the behavior of the deuteron form factor for very high q^2 ($|q^2| \gg M^2$). Also, our formulae may be expanded to zero and first order in q^2 , where they agree with known results.

As the description of our calculations is somewhat lengthy, we shall present our results at the outset. The next subsection gives our

numerical results and some conclusions; in particular, we show the deuteron structure functions for several models of the deuteron wavefunction. Section I-B examines the size of the relativistic effects, and Section I-C discusses the sensitivity of our results to the choice of nucleon form factor. Section I-D gives some analytic results for the behavior of the deuteron electromagnetic form factor at ultra-high q^2 . Section I-E contains comments upon the role of exchange currents in intermediate and high energy electron-deuteron elastic scattering, Section I-F compares our formulae, expanded to first order in q^2/M^2 , to previous results, and Section I-G estimates a theoretical uncertainty in this calculation. The full calculation is outlined in Section II.

A. Numerical results for different deuteron models

The main results are given in Figs. 2 through 11 which show various combinations of deuteron electromagnetic form factors for several different choices of the deuteron wavefunctions. In each graph, a solid line is inserted as a benchmark representing a nonrelativistic calculation using the Reid soft core wavefunction.⁵

In Figs. 2 through 6, we use our relativistic equations for the structure functions with wavefunctions calculated from a wave equation in which both nucleons were assumed to be on shell. The wavefunctions are the Holinde-Machleidt,⁶ the Lomon-Feshbach,⁷ and the Reid soft core⁵ wavefunctions, and the P-state wavefunctions are zero. These will be referred to collectively as two-component models.

In Figs. 7 through 11, the wavefunctions were themselves also calculated from a wave equation in which one of the nucleons is allowed to be off shell,⁸ and they are therefore completely consistent with our

formulae for the structure functions. (These relativistic wavefunctions are completely described in Ref. 8; briefly they are determined from a relativistic one boson exchange model with π , σ , ρ and ω exchanges, adjusted to give the correct deuteron binding energy and quadrupole moment. The π -NN vertex is a mixture of γ^5 and $\gamma^5\gamma^\mu$ couplings, with the mixing parameter λ defined so that the coupling is independent of λ when both nucleons are on shell, and is pure γ^5 when $\lambda = 1$ and pure $\gamma^5\gamma^\mu$ when $\lambda = 0$. The P-state wavefunctions are not zero, but turn out to increase nearly linearly with λ . These will be referred to collectively as four-component models.)

The A function shown in Figs. 2 and 7 and the B function shown in Figs. 3 and 8 are defined by the familiar equation,

$$\frac{d\sigma}{d\Omega} = \left. \frac{d\sigma}{d\Omega} \right|_{NS} [A(Q^2) + B(Q^2) \tan^2 \theta/2] \quad (1.1)$$

where

$$\left. \frac{d\sigma}{d\Omega} \right|_{NS} = \left(\frac{\alpha}{2E} \right)^2 \frac{\cos^2 \theta/2}{\sin^4 \theta/2} \frac{1}{\left[1 + \frac{2E}{M_d} \sin^2 \theta/2 \right]} \quad (1.2)$$

and $\alpha = e^2/4\pi \approx 1/137$, E is the energy of the incoming electron, θ the laboratory scattering angle of the electron, the deuteron mass is $M_d = 1.876$ GeV, q is the 4-momentum transferred by the electron, and we define $Q^2 = -q^2 > 0$ so that

$$Q^2 = \frac{4E^2 \sin^2 \theta/2}{1 + \frac{2E}{M_d} \sin^2 \theta/2} \quad . \quad (1.3)$$

The data shown on these curves is from Ref. 1.

The charge and quadrupole form factors, G_C and G_Q , together with the magnetic form factor G_M are defined in Section II, Eq. (2.9). The

relations between A and B and G_C , G_Q and G_M are

$$\begin{aligned} A(Q^2) &= G_C^2(Q^2) + \frac{Q^2}{6M_d^2} G_M^2(Q^2) + \frac{Q^4}{18M_d^4} G_Q^2(Q^2) \\ B(Q^2) &= \frac{Q^2}{3M_d^2} \left(1 + \frac{Q^2}{4M_d^2}\right) G_M^2(Q^2) \end{aligned} \quad (1.4)$$

In Figs. 4 and 5 and Figs. 9 and 10, the charge and quadrupole contributions to A, $G_C^2(Q^2)$ and $\left[Q^4/18M_d^4\right]G_Q^2(Q^2)$, are shown separately. Finally, the tensor polarization of the recoil nuclei when scattering from an unpolarized target is shown in Figs. 6 and 11. When this quantity⁹

$$T(Q^2) = \frac{\sqrt{2} Q^2}{3M_d^2} \cdot \frac{G_C G_Q + \frac{Q^2}{12M_d^2} G_Q^2}{G_C^2 + \frac{Q^4}{18M_d^4} G_Q^2} \quad (1.5)$$

is measured, one may be able to experimentally determine G_C and G_Q separately.

All curves in Figs. 2 through 16 were evaluated using isoscalar nucleon form factors given by the empirical dipole formulae with form factor scaling,

$$\begin{aligned} G_{ES} &= \frac{1}{[1 + Q^2/0.71]^2} \\ G_{MS} &= \frac{0.88}{[1 + Q^2/0.71]^2} \end{aligned} \quad (1.6)$$

where Q^2 is in $(\text{GeV}/c)^2$. The dependence of our results on the choice of form factor will be discussed in more detail in Section I-C.

As Figs. 2 and 7 show, all of the models lie below the data for A by a factor of 2-10, although the Lomon-Feshbach model gives larger structure than the other relativistically calculated models. The reason this model is so much larger than the others can be traced to the discontinuity in the S-state wavefunction (see Fig. 12), which introduces large oscillations in momentum space which keep the wavefunction large at high momentum.

There are two immediate questions: how has the relativistic calculation changed the non-relativistic result and why are the results consistently low? We discuss these questions in turn.

B. Size of the relativistic corrections

One of the major goals of this calculation was to gain some understanding of the size and nature of the relativistic effects. This can be provided by a detailed examination of Figs. 13-16, which we will discuss now in some detail.

In Figs. 13 and 14, we have displayed the relativistic corrections for the two-component models presented in Figs. 2-6, while Figs. 15 and 16 display the relativistic corrections for the four-component models presented in Figs. 7-11.

In Fig. 13, we have displayed the ratio of the relativistic calculation of A given in Fig. 2 to the non-relativistic calculation for each of the models considered in Fig. 2. The figure shows that use of the relativistic formulae tends to reduce the theoretical value of A by a factor of 2-5 at about $100 F^{-2}$, and that except for the Lomon-Feshbach models, all of the non-relativistic models tend to give about the same correction out to about $60 F^{-2}$. In Fig. 14, we have displayed the

relativistic effects on each of the fundamental form factors individually. Here we found it more illuminating to display the difference ΔG between the relativistic and non-relativistic results, and because the curves vary considerably, we have shown the differences for all the models in Figs. 14(b), 14(d) and 14(f), but the individual relativistic and non-relativistic results from which differences are calculated are displayed only for the HM3 model⁶ in Figs. 14(a), 14(c) and 14(e).

Note that both the form factors and the differences tend to oscillate, but in such a way that in all cases the effect of the relativistic corrections is to shift the diffraction minima to lower Q^2 with a corresponding increase in the following maxima.

In Figs. 15 and 16, we have displayed the relativistic corrections for the relativistic models of Ref. 8. The principal differences between the results in these figures and those in Figs. 13 and 14 is due to the presence of the P-states, which contribute additional corrections. The final formulae have terms linear in the P-states (i.e., interference terms between the P-states and either an S or D state) and quadratic in the P-states, as well as terms independent of the P-states. Any of the structure functions could therefore be calculated in four different ways: (1) non-relativistically using only the u and w wavefunctions from the 4-component model, (2) relativistically, but using only the u and w wavefunctions, (3) relativistically, but excluding the terms quadratic in the P-states (so that only terms independent of the P-states or linear in the P-states are included), and (4) the full result obtained by inserting all four wavefunctions in the relativistic formulae. (In the first three cases, the u and w wavefunctions must be rescaled to

satisfy the non-relativistic normalization condition.) For the A structure function, the first case is called A_{NR} , the second A_{None} (for no P-states), the third is A_{Lin} (linear in the P-states) and the fourth A_{Full} , and information about all of these ways of computing A is presented in Fig. 15. In Fig. 15(a), the ratio $R_{Full} = A_{Full}/A_{NR}$ is presented for each of the three models considered in Figs. 7-11; this gives the total result of including all relativistic effects. Figure 15(b) also includes two other ratios for the $\lambda = 1$ model: $R_{None} = A_{None}/A_{NR}$ and $R_{Lin} = A_{Lin}/A_{NR}$.

The ratio R_{None} shows that if the P-states are ignored, the relativistic corrections are very similar to the results obtained from the two-component models. Comparison R_{Lin} and R_{Full} (for the $\lambda = 1$ case) with R_{None} shows that adding the P-states introduces a sizable change in the results and that the effect of the terms quadratic in the P-states is somewhat smaller than the linear terms, as one might expect. Comparison of the R_{Full} ratios for the three models shows considerable model dependence, reflecting the fact that the P-states are very tiny for $\lambda = 0$ and increase as λ goes from 0 to 1.

Figure 16 shows the relativistic effects on each of the fundamental form factors. In Figs. 16(a), 16(c) and 16(e), we have presented, for the $\lambda = 1$ model, each of the four possible cases discussed above, labeled NR, None, Lin and Full, together with the difference between the Full result and the NR result. The other parts, Figs. 16(b), 16(d) and 16(f), show the differences between the Full and NR results for each of the three models. We can see from these figures that the total effect of the relativistic corrections is to shift the diffraction minima to lower values of Q^2 (just as we found before) for G_C and G_Q (when $\lambda = 0$ or .4),

but that for G_M (and G_Q when $\lambda = 1$) we have the opposite effect -- the corrections shift the minima to higher Q^2 . These trends are a result of two competing effects: the relativistic kinematics, which tends to shift all diffraction minima to lower Q^2 as we observed before, and the P-states, which tend to have the opposite effect. For the electric form factors, G_C and G_Q , the P-state effects tend to be suppressed, so that only when they are exceptionally large ($\lambda = 1$) do they have a significant effect, changing the direction of the shift in G_Q (where the linear and quadradic P-state terms have the same sign) and significantly reducing the shift in G_C (where the linear and quadradic P-state terms tend to cancel). In G_M , the P-state contributions are less suppressed, so that the sign of the shift is opposite for all cases.

We now summarize the observations that can be made from the numerical results presented in these two parts:

(i) The relativistic corrections to A are significant at large Q^2 .

The "conventional" two-component models and the four-component models with $\lambda = 0$ (pure $\gamma^5 \gamma^\mu$ coupling for the pion) tend to give very similar corrections out to about $60 F^{-2}$, and these corrections depress the non-relativistic results and widen the difference between the data and the theory. The Lomon-Feshbach models, which are unconventional because they have discontinuities in the wavefunction, and the four-component model with $\lambda = 1$ (pure γ^5 coupling for the pion) give different corrections which are smaller and which can be positive in the intermediate region of Q^2 around $40 F^{-2}$.

(ii) Since the four component models with different λ give relativistic corrections to A which differ significantly from each other,

we conclude that these corrections are sensitive to the form of the pion nucleon coupling in disagreement with what might be expected on the basis of a naive application of the equivalence theorem.¹⁰ Furthermore, one should have some confidence in this conclusion since the three four-component deuteron models we used are very closely related,⁸ and because our calculation includes, in a completely unified manner,¹¹ what other investigators often calculate separately as relativistic effects,¹² renormalization corrections,¹³ and "pair" current corrections.¹⁴

(iii) Using the dipole formula for the nucleon form factors, none of the models do a satisfactory job of fitting the data for the A structure function. The results are systematically low. One explanation for this is that there are sizable contributions to electron deuteron elastic scattering from processes that we have not included, such as the iso-scalar meson exchange process illustrated in Fig. 1(c) and scattering from isobar currents as in Fig. 1(d). Others have found that the contribution from the $\rho\pi\gamma$ exchange current, in particular, can be quite significant^{14,15} in this Q^2 range, while the contributions from the isobar currents are predicted to be small.¹⁶ Neither of these processes has been calculated to all orders in q^2/M^2 .

(iv) The meson exchange currents are not necessarily the only explanation for the discrepancy. In particular, G_{En} is not well known. The A structure function is more sensitive to $G_{ES} = G_{Ep} + G_{En}$ than to $G_{MS} = G_{Mp} + G_{Mn}$, and goes approximately as G_{ES}^2 . We have used $G_{En} = 0$; but a value of G_{En} twice as large and of the same sign as G_{Ep} at Q^2 of 3 (GeV/c)^2 is not inconsistent with any data and would enhance $A(Q^2)$ by an order of magnitude. When the meson exchange and isobar current con-

tributions have been calculated to all orders in q^2/M^2 , our theory may be sufficiently reliable to permit extraction of G_{En} from the data for A .

Further discussion of the role of the exchange currents appears below in Section I-E, following the analytic discussion of the behavior of the structure functions at ultrahigh Q^2 in Section I-D. In the next section we discuss the uncertainties introduced by our lack of knowledge of the nucleon form factors.

C. The nucleon electromagnetic form factors

Thus far, all of the results presented have used dipole nucleon electromagnetic form factors with form factor scaling as in Eq. (1.6) with G_{En} set equal to zero. The nucleon form factors, however, are not well measured quantities. The proton magnetic form factor G_{Mp} is the best known with uncertainties of 3% to 5% in the Q^2 range up to 10 $(\text{GeV}/c)^2$, and there is data¹⁷ up to Q^2 of 33 $(\text{GeV}/c)^2$. Measurements of G_{Ep} extend¹⁸ only to 3 $(\text{GeV}/c)^2$, where the uncertainty is nearly 100%. The neutron form factors are even less well known. The magnetic form factor G_{Mn} has been measured¹⁹ up to 2 $(\text{GeV}/c)^2$ with uncertainties ranging from 10% to 40%. The neutron electric form factor G_{En} is the least well known. It has been deduced in model dependent analyses of quasielastic and elastic electron scattering²⁰ from deuterium only out to Q^2 of 1 $(\text{GeV}/c)^2$. The errors are large, 30% to 50%, but G_{En} seems to have a positive value of approximately .05 in the Q^2 range 0.2 to 1 $(\text{GeV}/c)^2$. The slope of G_{En} at $Q^2 = 0$, obtained by scattering neutrons from atomic electrons,²¹ is positive and is known to better than 3%.

To see how sensitive the deuteron structure functions are to reasonable choices for the nucleon structure functions, we have prepared plots in Figs. 17-20 of A and B calculated using five different sets of nucleon form factors. In Fig. 21 the various curves for G_{En} used in this paper are plotted together with the dipole form for G_{Ep} .

The curves labeled IJL were calculated using the form factors from Ref. 22. They were obtained from a fit to the world's data for G_{Ep} , G_{Mp} and G_{Mn} using a vector dominance model. In general, this fits the proton data well, but it gives results for the neutron that, in our judgment, look unreasonable, particularly for G_{En} (which was not included in the fit). The IJL parameterization gives a curve for G_{En} that goes negative at Q^2 of 1.4 (GeV/c)^2 . Above approximately 3 (GeV/c)^2 G_{En} has an absolute value comparable to G_{Ep} and thus G_{Es} becomes very small. Therefore, the A and B structure functions show a sharp minimum in that region of Q^2 (see Figs. 17-20) due to this cancellation of the nucleon form factors in addition to the usual diffraction features in the fundamental form factors.

To display results for what we regard as more reasonable neutron form factors, we have assembled a collection we call "Best Fit", first used in Ref. 1. While they are not obtained from a comprehensive fit to all the form factors simultaneously, in each case there is good agreement with the present limited data. The proton form factors are those of IJL.²² The neutron G_{Mn} is taken from a fit by Hansen *et al.*,¹⁹ and for G_{En} we use a formula suggested by Galster *et al.*,²⁰

$$G_{En} = \frac{-\mu_n \tau}{1 + 5.6\tau} G_{Ep} \quad (1.7)$$

where μ_n is the neutron magnetic moment, $\tau = Q^2/4M_n^2$, and for G_{Ep} we have taken the IJL values. (Galster et al.²⁰ used the dipole form for G_{Ep} .)

To display the sensitivity of A and B to G_{En} we have also plotted in Figs. 17-20 curves in which the Best Fit form factors were used, except that G_{En} was set equal to zero, and the curves are labeled "Best Fit + $G_{En} = 0$." When these curves are compared to the dipole curves, they also show the effect of possible variations in G_{Ep} .

Finally, the curve labeled "Dipole + $F_{1n} = 0$ " is an attempt to indicate what possible form G_{En} could take to give agreement with the data for $A(Q^2)$. This curve employs the usual dipole forms, except that the neutron Dirac form factor is set equal to zero. This assumption is consistent with the prediction of the symmetric quark model for the nucleon structure where the valence quarks are all in a spacially symmetric ground state²³ and gives:

$$G_{En} = \tau G_{Mn} = -\mu_n \tau G_{Ep} \quad . \quad (1.8)$$

This parameterization was also considered by Galster et al.,²⁰ and it gives a value for G_{En} which is about a factor of two higher than the Best Fit value, and is at the upper edge of the large experimental error bars in the Q^2 range up to 1 (GeV/c)^2 . Therefore, it is a plausible estimate for G_{En} and is used here simply to give an idea of the size and shape of a G_{En} that might be required to explain the discrepancy between the RIA and the data for $A(Q^2)$, assuming for the moment that other possible mechanisms, such as meson exchange currents, are not present.

If we ignore the IJL curves and consider only the Dipole and the two Best Fit curves, we see in each case the curves for $A(Q^2)$ lie below the data by as much as a factor of ten. The spread in values, mainly due to different values for G_{En} , is less than a factor of two. This spread is about the same size as that due to different deuteron models, excluding the Feshbach-Lomon models, as shown in Figs. 2-11. The discrepancy with the data has been increased by making the calculations completely relativistic, as pointed out above.

A major task, then, is to explain this rather large disagreement between the RIA and the data. The favorite mechanism suggested as the possible source of the extra cross-section needed is the possibility of scattering from meson exchange currents. It is clear the meson exchange current processes must also be included and calculated to all orders in q^2/M^2 as are the impulse contributions in our treatment before the comparison with the data can be used to deduce information either about deuteron wavefunctions or nucleon form factors. However, in the meantime, we can see from Figs. 17 and 19 that it is possible that at least some of the difference between the RIA and the data might be due to using values for the neutron form factor G_{En} which are too small. The curve where F_{1n} was set to zero are seen to pass nearly through the data over the entire Q^2 range for the HM3 wavefunction and to give much improved agreement with the data for the $\lambda = 0.4$ wavefunction.

D. Behavior of the form factor at ultrahigh momentum transfer

In the ultrarelativistic region $Q^2 = -t \gg 4M_d^2$, our results can be analytically expanded and the leading term in a power series expansion M_d^2/Q^2 can be obtained. This is of considerable importance for comparison

with the quark model^{24,25} and to assess the importance of meson exchange effects^{14,15} at high Q^2 .

The actual calculations are in Section II-E, and we shall just make some comments and state the results here. The high momentum transfer behavior of the form factor depends upon the high momentum behavior of the vertex function or wavefunctions. If we assume that the wavefunctions go like p^{-N} , where p is the magnitude of the relative momentum, and that the nucleon form factors go like t^{-2} , then the deuteron structure functions go like

$$\begin{aligned} A(t) &\rightarrow t^{-(3+2N)} \\ B(t) &\rightarrow t^{-(2+2N)} \end{aligned} \tag{1.9}$$

so that if we define an angle dependent form factor by

$$\frac{d\sigma}{d\Omega} = \frac{d\sigma}{d\Omega} \Big|_{NS} F_d^2(t, \theta) = \frac{d\sigma}{d\Omega} \Big|_{NS} [A(t) + B(t) \tan^2 \theta/2] \tag{1.10}$$

then at fixed angle,

$$F_d^2(t, \theta) \rightarrow t^{-(2+2N)} \tag{1.11}$$

and the $B(t)$ or purely magnetic term dominates $A(t)$.

The power N at which the wavefunctions go to zero at large p can be determined by studying²⁶ the (covariant) wave equation which one uses to solve for the deuteron vertex function. We use the formulation where one nucleon is restricted to the mass shell,⁴ and we suppose that the binding is given by a series of one boson exchanges with each BNN vertex having a form factor which goes like $(r^2 + p_1^2 + p_2^2)^{-\epsilon}$, where r is the momentum transfer through the boson and p_1 and p_2 are the nucleon four-momenta. If the BNN couplings include no momentum dependent terms like

$\gamma^5 \gamma^\mu$, or $\sigma^{\mu\nu} q_\nu$, then it is reasonable to choose $\epsilon = 1$,²⁷ while if there are such momentum dependent terms, $\epsilon = 3/2$ would ensure the same asymptotic behavior. In these cases, one would obtain $N = 4$, and

$$\begin{aligned} A(t) &\rightarrow t^{-11} \\ B(t) &\rightarrow t^{-10} \\ F_d^2(t, \theta) &\rightarrow t^{-10} \end{aligned} \quad (1.12)$$

To compare our results with the quark model, we must be careful to remember that the quark model results are usually stated for the limit when t becomes large with s/t fixed. (This was overlooked in Ref. 2 leading us to an erroneous conclusion.) Using the relationship

$$\tan^2 \theta/2 = \frac{-M_d^2 t}{(s - M_d^2)^2 + (s - M_d^2)t - M_d^2 t} = \frac{M_d^2}{-t} f_1(t/s) \quad (1.13)$$

(where the last part is true for $s \gg M_d^2$ and c.m. scattering angle not directly backward), we obtain

$$F_d^2 \xrightarrow[s/t \text{ fixed}]{} t^{-(3+2N)} \rightarrow t^{-11} \quad . \quad (1.14)$$

Since the quark model predicts a t^{-10} behavior for this quantity, we see that the RIA falls faster than the quark model at large t . This has implications for the role of exchange currents, which we will discuss in the next section.

E. The role of exchange currents

Before the experiment of Ref. 1, meson exchange currents were expected to dominate elastic e-d scattering at momentum transfers above

1 (GeV/c)^2 . Since the data turned out much smaller than predicted by the early meson exchange calculations,¹⁵ there has been some confusion about their ultimate role.

First, we wish to clearly distinguish between the so-called pair currents, illustrated in the last two diagrams of Fig. 1(b), and terms in which the photon couples directly to mesons, as shown in Fig. 1(c). When four-component wavefunctions are used this calculation consistently incorporates all contributions from pair currents, which we find it helpful to regard as relativistic effects. In this part our discussion will be directed only toward the true exchange currents of the type shown in Fig. 1(c), not included in this calculation.

Our discussion should also distinguish between asymptotic Q^2 and currently feasible experimental Q^2 . At asymptotic Q^2 , we have seen that the quark model predicts a different and slower falloff with Q^2 than the RIA. If the quark model result correctly describes ultrahigh Q^2 e-d scattering, then the impulse approximation cannot play an important role at those momentum transfers, and one can argue that, in nuclear physics terms, the exchange currents dominate. We remind the reader that the pair currents are properly included in the RIA, and this means that they cannot be among the dominating terms at asymptotic Q^2 .

The Q^2 region of the American University -- SLAC experiment¹ is, however, not at asymptotic Q^2 , defined by the condition $Q^2 \gg 4M_d^2 \approx 16 \text{ (GeV/c)}^2$. However, the exchange currents may already be important, particularly since our own calculations do not saturate the data. However, reaching definite conclusions about the size of the exchange currents by subtracting our calculation from the data should require

better independent knowledge of the deuteron wavefunction and, especially, of the neutron charge form factor. While it is now clear that the early calculations¹⁵ were too large because they omitted form factors at the nucleon vertices and used couplings that were in some cases too large, recent calculations¹⁴ suggest that the $\rho\pi\gamma$ contribution is nevertheless large above 2 (GeV/c)^2 . However, in the RIA the full calculation differs significantly from a calculation that includes terms only to order Q^2/M_d^2 , so we feel that the exchange current calculations also need to be done fully relativistically.

F. Low Q^2 results

In Section II we show that when $(Q/M)^2$ is small, our formulae reduce to the correct nonrelativistic limit. In addition to the usual integrals over products of S and D-state wavefunctions, we also obtain terms corresponding to overlap between these wavefunctions and the P-state wavefunctions, and terms corresponding to products of P-state wavefunctions. At $Q^2 = 0$ these terms give corrections to both the magnetic moment and the quadrupole moment. Most of these results have been obtained previously by other investigators^{12,28} but we shall record here the magnetic moment and quadrupole moment formulae since the corrections due to the extra parts of the wavefunction may be larger than the experimental errors in the measurement:

$$\begin{aligned}
 \mu_d &= (1 + \tilde{F}_2) \left(1 - \frac{3}{2} p_d - \frac{3}{2} p_{v_t} - p_{v_s} \right) \\
 &+ \frac{3}{4} p_d + \frac{1}{4} p_{v_t} - \frac{1}{2} p_{v_s} - \sqrt{2} \tilde{F}_2 \int_0^\infty dr v_t v_s \\
 &+ \frac{1}{\sqrt{6}} \int_0^\infty dr Mr \left\{ v_t (u - \sqrt{2} w) - v_s (\sqrt{2} u + w) \right\} + \Delta_\mu \quad (1.15)
 \end{aligned}$$

$$\begin{aligned}
 \frac{M_d^2}{4M^2} Q_d &= \frac{\sqrt{2}}{10} \int_0^\infty r^2 dr \left[uw - \frac{w^2}{\sqrt{8}} + \frac{v_t^2}{\sqrt{8}} - \frac{v_s^2}{\sqrt{2}} \right] \\
 &+ \left[2\tilde{F}_2 + 1 \right] \frac{1}{\sqrt{3}} \int_0^\infty \frac{r dr}{2M} \left[u \left(v_s + \frac{1}{\sqrt{2}} v_t \right) - \frac{1}{5} w \left(2v_t + \frac{1}{\sqrt{2}} v_s \right) \right] + \Delta_Q \quad (1.16)
 \end{aligned}$$

where $\tilde{F}_2 = (\mu_p + \mu_n - 1) \frac{M_d}{2M}$, μ_p and μ_n are the proton and neutron magnetic moments, Δ_μ and Δ_Q are additional corrections of order p^2/M^2 , given in Section II, Eq. (2.77), and

$$\begin{aligned}
 p_d &= \int_0^\infty w^2 dr \\
 p_{v_s} &= \int_0^\infty v_s^2 dr \\
 p_{v_t} &= \int_0^\infty v_t^2 dr \quad . \quad (1.17)
 \end{aligned}$$

We can also very easily obtain the corrections to first order in Q^2/M^2 to the charge and quadrupole form factors from our formulae, and these are given in Section II. It is not surprising that the part of our result for those terms which comes from products of the S and D-state wavefunctions is identical to that obtained earlier by Gross²⁹ using the same general method that we use here. Friar¹² and Coester and Ostebee²⁸ use a different technique, but the calculation of Coester and Ostebee and our calculation agree precisely and both have some terms proportional to the potential not included by Friar. However, it has recently been shown¹¹ that the extra "potential" terms we obtain correspond to renormalization corrections and part of the "pair" current corrections if one uses the framework employed by Friar, and that when one adds the terms linear in the P-states, our corrections to first order in Q^2/M^2 agree with the sum of Friar's relativistic corrections, the renormalization corrections of Gari and Hyuga,¹³ and the "pair" current corrections.¹⁴ Hence, it now appears that both approaches agree to first order in Q^2/M^2 as long as one is careful to include all of the effects.

The advantage of our approach, however, is that we automatically include corrections to all orders in Q^2/M^2 . In Fig. 22, we have compared our result with the Q^2/M^2 expansion for the Reid soft core wavefunction. Note that the "potential" terms make the largest contributions (as observed by Coester and Ostebee²⁸) and that the Q^2/M^2 expansion follows the full result out to about $80 F^{-2}$. The "argument" shift proposed by Friar some time ago is also shown for comparison.

We conclude that if one does not require a precise theory, the first two terms in a Q^2/M^2 expansion will probably be sufficient for Q^2 below about $80 F^{-2}$, but that a precise calculation requires the full theory even at lower Q^2 .

G. Estimate of a theoretical uncertainty

Our calculation of the RIA makes the approximation that the spectator nucleon is on shell. In this section we will estimate the error involved in this approximation and will see that the error is about the size of the terms quadratic in the P-state wavefunctions and small compared to, e.g., the differences that result from using different wavefunctions.

The simplest way to make the estimate is to work with a scalar deuteron made from two scalar nucleons. In this case, the d-n-p vertex is described by only one scalar function Γ , which we shall treat as a constant. We begin with the triangle diagram as in Fig. 1(a), and allow the spectator to be off shell, so that

$$2D_0 G(Q^2) = i F(Q^2) \int \frac{d^4 p}{(2\pi)^4} \Gamma^2 \frac{2(D_0 - p_0)}{(p^2 - M^2)((D-p)^2 - M^2)((D'-p)^2 - M^2)} \quad (1.18)$$

where $F(Q^2)$ is the isoscalar nucleon form factor, and we work in the Breit frame

$$D = (D_0, -\frac{1}{2} \vec{Q}) \quad ; \quad D' = (D_0, +\frac{1}{2} \vec{Q}) \quad . \quad (1.19)$$

Doing the integral in p_0 by the residue theorem gives three terms, and after combining the two terms which come from the interacting nucleon

poles we get

$$\begin{aligned}
 G(Q^2) &= \frac{F(Q^2)}{2D_0} \int \frac{d^3 p}{(2\pi)^3} \Gamma^2 \left\{ \frac{D_0 - E}{E[(D_0 - E)^2 - E_+^2][(D_0 - E)^2 - E_-^2]} \right. \\
 &\quad \left. + \frac{2D_0 + E_+ + E_-}{(E_+ + E_-)[(D_0 + E)^2 - E^2][(D_0 + E_-)^2 - E^2]} \right\} \quad (1.20)
 \end{aligned}$$

where $E = E(\vec{p}) = (M^2 + p^2)^{1/2}$, and $E_{\pm} = E(\vec{p} \pm \frac{1}{2}\vec{Q})$. The first term comes from the spectator pole and is the term we have kept in our calculation; the second term is the correction. The second term is of order p^4/M^4 compared to the first term.

Finally, it can be seen from the definitions of the wavefunctions that the P-state parts are typically of order p^2/M^2 compared to the S-state contributions (see Section II). (One might also see this directly above by decomposing the interacting nucleon propagators in the first term above into positive and negative energy propagators in some appropriate reference frame. The former give the analog of the usual S-states and the latter give the analog of the P-states and are clearly smaller by a factor p^2/M^2 .) Therefore, one expects the correction or the uncertainty to be of the order of the size of the contributions quadratic in the P-states. A glance at Fig. 15(b) shows that the correction is roughly of the size of the difference between $(A_{\text{Full}}/A_{\text{NR}})$ and $(A_{\text{Lin}}/A_{\text{NR}})$, which is not negligible, but which is nevertheless smaller than other effects at low Q^2 . The uncertainty is about 10% at $Q^2 \simeq 4 \text{ (GeV)}^2$.

II. The Calculation

We now turn to a description of the details of the calculation.

This section is divided into 7 parts: (A) Kinematics, (B) The Relativistic Impulse Approximation (RIA), (C) The Matrix Elements of the Current, (D) The Final Formulae, (E) The Ultrahigh q^2 Limit, (F) The Formulae for Low q^2 , and (G) Numerical Evaluation of the Integrals.

A. Kinematics

The matrix element of elastic e-d scattering is³⁰

$$\mathcal{M} = e^2 \frac{\bar{u}(k') \gamma^\mu u(k)}{q^2} G_\mu(q^2) \quad (2.1)$$

where u and \bar{u} are fermion spinors and k and k' are the 4-momenta of the initial and final electrons; D and D' will be the 4-momenta for the initial and final deuterons. Also

$$q_\mu \equiv (D' - D)_\mu \quad (2.2)$$

and

$$-q^2 = -(D' - D)^2 \equiv Q^2 \geq 0 \quad (2.3)$$

The interaction of the deuteron with the virtual photon is fully described by the vector function G^μ , which can be decomposed into 3 scalar functions according to³¹

$$\begin{aligned} G^\mu(q^2) = & - \left\{ G_1(q^2) (\xi'^* \cdot \xi) (D + D')^\mu \right. \\ & + G_2(q^2) [\xi^\mu (\xi'^* \cdot q) - \xi'^* \cdot \xi (q \cdot q)] \\ & \left. - G_3(q^2) \frac{(\xi \cdot q) (\xi'^* \cdot q) (D + D')^\mu}{2M_d^2} \right\} \end{aligned} \quad (2.4)$$

Here ξ and ξ' are polarization 4-vectors for the incoming and outgoing deuterons, respectively, and satisfy

$$\xi \cdot D = \xi' \cdot D' = 0 \quad . \quad (2.5)$$

It will be convenient to do much of our calculation in the Breit frame, where

$$q = (0, \vec{Q})$$

$$D = (D_0, -\frac{1}{2}\vec{Q})$$

$$D' = (D_0, +\frac{1}{2}\vec{Q})$$

$$D_0 = \left(M_d^2 + \frac{1}{4}Q^2 \right)^{\frac{1}{2}} \quad (2.6)$$

and we choose \vec{Q} to be in the positive z direction. Note that because of the convention (2.3) Q^2 is both the negative of the square of the 4-momentum transfer and the square of the 3-momentum transfer in the Breit frame, and Q will always represent $|\vec{Q}|$. In this frame, the three polarization states of the incoming deuteron are

$$\xi^\mu(\pm 1) = (0, \mp 1, -i, 0) / \sqrt{2}$$

$$\xi^\mu(0) = (-Q, 0, 0, D_0) / M_d \quad (2.7)$$

where the argument of the ξ refers to the component of the spin in the z direction and not to the helicity.

In the Breit frame G^μ can be rewritten in terms of quantities with a non-relativistic appearance if we introduce rest frame polarization vectors

$$\xi_0^\mu(\pm 1) = \xi^\mu(\pm 1)$$

$$\xi_0^\mu(0) = (0, 0, 0, 1) . \quad (2.8)$$

Then, in the Breit frame,

$$\begin{aligned} G^0(q^2) &= 2D_0 \left\{ (\vec{\xi}'_0 \cdot \vec{\xi}_0) G_C(q^2) \right. \\ &+ \left. \left[(\vec{\xi}'_0 \cdot \vec{Q}) (\vec{\xi}_0 \cdot \vec{Q}) - \frac{1}{3} \vec{Q}^2 (\vec{\xi}_0 \cdot \vec{\xi}'_0) \right] \frac{G_Q(q^2)}{2M_d^2} \right\} \end{aligned}$$

$$\vec{G}(q^2) = \frac{D_0}{M_d} \left[\vec{\xi}_0 (\vec{\xi}'_0 \cdot \vec{Q}) - \vec{\xi}'_0 (\vec{\xi}_0 \cdot \vec{Q}) \right] G_M(q^2) \quad (2.9)$$

where we have used the charge, magnetic, and quadrupole form factors

$$\begin{aligned} G_C &= G_1 + \frac{2}{3} \eta G_Q \\ G_M &= G_2 \\ G_Q &= G_1 - G_2 + (1 + \eta) G_3 \end{aligned} \quad (2.10)$$

where $\eta = Q^2/4M_d^2$, $G_C(0) = 1$, $G_M(0) = \mu_d$ in units $(2M_d)^{-1}$, and $G_Q(0) = Q_d$ in units M_d^{-2} . As we do our calculation, Eq. (2.9) will be useful in letting us pick out G_C , G_M and G_Q directly.

Also in this section we will collect a few formulae related to what we call the relativistic deuteron wavefunction, or, more precisely, the bound state Bethe-Salpeter wavefunction with one leg on shell. Consider a deuteron with momentum D and polarization ξ breaking into nucleons of momentum p and $D-p$, conserving energy and momentum. The momentum p is to be on shell, $p^2 = M^2$, forcing the other nucleon to be off shell,

$(D-p)^2 \neq M^2$. The d-n-p vertex function and the deuteron wavefunction are defined by

$$\begin{aligned} \langle ps | \psi(0) | D\xi \rangle &= \frac{[M + \gamma \cdot (D-p)] \Gamma^\lambda(p, D) \xi_\lambda c \bar{u}^T(p, s)}{\sqrt{(2\pi)^3 2D_0} (M^2 - (D-p)^2)} \\ &= \psi^\mu(p, D) \xi_\mu . \end{aligned} \quad (2.11)$$

The first line defines the Blankenbecler-Cook³ d-n-p vertex function, Γ , which is a 4×4 matrix in dirac space and is a function either of D and P or equivalently of D and the relative momentum p_{rel} ,

$$p_{\text{rel}} = p - \frac{1}{2} D . \quad (2.12)$$

We will specify the vertex function further only to note that four scalar functions are imbedded within it:

$$\Gamma^\mu = F\gamma^\mu + \frac{G}{M} p_{\text{rel}}^\mu - \left(\frac{M - \gamma \cdot (D-p)}{M} \right) \left[H\gamma^\mu + \frac{I}{M} p_{\text{rel}}^\mu \right] \quad (2.13)$$

F, G, H and I are functions of p_{rel}^2 , and our results could be written in terms of them, but we have chosen instead to use four equivalent functions now to be defined and whose nonrelativistic analogs are obvious.

Equation (2.11) defines the wavefunction,⁴ which as written above has two suppressed indices, one dirac index for the off-shell nucleon and one spin index s for the on-shell nucleon. In the rest frame of the deuteron $\vec{D} = 0$, $\vec{p}_{\text{rel}} = \vec{p}$, and we define

$$\psi_{s\alpha}^\lambda(p, M_d) \xi_{0\lambda} = \sum_r \left\{ \psi_{sr}^+(\vec{p}) u_\alpha(-\vec{p}, \vec{r}) + \psi_{sr}^-(\vec{p}) v_\alpha(\vec{p}, -\vec{r}) \right\} \quad (2.14)$$

where M_d can be a shorthand for the 4-vector $(M_d, \vec{0})$.

This definition was motivated by the observation that the propagation of an off-shell particle (momentum \vec{p}) can be viewed as a superposition of positive and negative energy on-shell states. (If $D-p$ could be on-shell, the second term would be absent.) Using the decomposition

$$\frac{M + \gamma \cdot (M_d - p)}{M^2 - (M_d - p)^2} = \frac{M}{E_p} \sum_r \left\{ \frac{u(-\vec{p}, r) \bar{u}(\vec{p}, r)}{2E_p - M_d} - \frac{v(\vec{p}, -r) \bar{v}(\vec{p}, -r)}{M_d} \right\} \quad (2.15)$$

where $E_p = (M^2 + \vec{p}^2)^{\frac{1}{2}}$, we get (still in the rest frame)

$$\begin{aligned} \psi_{sr}^+(\vec{p}) &= \frac{M}{\sqrt{(2\pi)^3 2M_d}} \frac{\bar{u}(-\vec{p}, r) \xi_0^\mu \Gamma_\mu(p, M_d) C \bar{u}^T(\vec{p}, s)}{E_p (2E_p - M_d)} \\ \psi_{sr}^-(\vec{p}) &= \frac{-M}{\sqrt{(2\pi)^3 2M_d}} \frac{\bar{v}(\vec{p}, -r) \xi_0^\mu \Gamma_\mu(p, M_d) C \bar{v}^T(\vec{p}, s)}{E_p M_d} \end{aligned} \quad (2.16)$$

Now a small amount of manipulation allows us to define the four wavefunctions that we will use in stating our final results. We have^{4,8}

$$\begin{aligned} \psi_{sr}^+(\vec{p}) &= \frac{1}{\sqrt{8\pi}} \left[\left(u(p) - \frac{1}{\sqrt{2}} w(p) \right) \vec{\sigma} \cdot \vec{\xi}_0 + \frac{3}{\sqrt{2}} w(p) \vec{\sigma} \cdot \hat{p} \hat{p} \cdot \vec{\xi}_0 \right] (i\sigma_2) \Big|_{rs} \\ \psi_{sr}^-(\vec{p}) &= \frac{1}{\sqrt{8\pi}} \left[-\sqrt{\frac{3}{2}} v_t(p) i\vec{\sigma} \cdot \hat{p} \times \vec{\xi}_0 + \sqrt{3} v_s(p) \hat{p} \cdot \vec{\xi}_0 \right] (i\sigma_2) \Big|_{rs} \end{aligned} \quad (2.17)$$

where u and w are the familiar momentum space S and D-state wavefunctions and v_t and v_s are the spin triplet and singlet P-state wavefunctions, respectively. Care should be taken to observe that the matrix indices

on the RHS of the equation are reversed from those on the left-hand side. The numerical factors have been chosen to give the momentum space normalization

$$\int_0^\infty p^2 dp (u^2 + w^2 + v_t^2 + v_s^2) = 1 . \quad (2.18)$$

The Fourier transforms are

$$\begin{aligned} \frac{u(r)}{r} &= \sqrt{\frac{2}{\pi}} \int_0^\infty p^2 dp j_0(pr) u(p) \\ \frac{w(r)}{r} &= \sqrt{\frac{2}{\pi}} \int_0^\infty p^2 dp j_2(pr) w(p) \\ \frac{v_{t,s}(r)}{r} &= \sqrt{\frac{2}{\pi}} \int_0^\infty p^2 dp j_1(pr) v_{t,s}(p) , \end{aligned} \quad (2.19)$$

and in coordinate space

$$\int_0^\infty dr (u^2 + w^2 + v_t^2 + v_s^2) = 1 . \quad (2.20)$$

B. The relativistic impulse approximation (RIA)

The calculation is based on the diagram shown in Fig. 1(a). The full diagram is

$$\begin{aligned} G^\mu(q^2) = -i \int \frac{d^4 p}{(2\pi)^4} \text{tr} \left\{ \frac{(M+p^T)}{M^2 - p^2 - i\epsilon} C \tilde{\Gamma}^\nu(p', D') \xi_\nu^{*\dagger} \frac{M+p' - p}{M^2 - (D'-p')^2 - i\epsilon} \right. \\ \left. F^\mu \frac{M+p - p'}{M^2 - (D-p)^2 - i\epsilon} \Gamma^\lambda(p, D) \xi_\lambda C \right\} \end{aligned} \quad (2.21)$$

where C is the Dirac charge conjugation matrix, F^μ the isoscalar nucleon current

$$F^\mu = F_{1S}(q^2) \gamma^\mu + \frac{i\sigma^{\mu\nu}}{2M} q_\nu F_{2S}(q^2) \quad (2.22)$$

where F_{1S} and F_{2S} are the Dirac and Pauli isoscalar form factors normalized so that

$$\begin{aligned} F_{1S}(0) &= 1 \\ F_{2S}(0) &= -0.12 \end{aligned} \quad (2.23)$$

and Γ is the deuteron-nucleon vertex function for the incoming deuteron. The vertex function for the outgoing deuteron can be computed from that for an incoming deuteron by

$$\Gamma \rightarrow \tilde{\Gamma} = \gamma^0 \Gamma^\dagger \gamma^0 \quad (2.24)$$

To obtain our starting formula, we perform the integration over p_0 , retaining only the positive energy pole from the spectator. The validity of this approximation has been discussed elsewhere³² and in Section I-G. We next substitute the relativistic deuteron wavefunction defined in Eq. (2.11) to obtain

$$\begin{aligned} G^\mu(q^2) &= 2D_0 \int d^3 p \frac{M}{E_p} \bar{\psi}_{s\alpha}^\nu(p', D') \xi_\nu'^* \\ &F_{\alpha\alpha'}^\mu \psi_{s\alpha'}^\lambda(p, D) \xi_\lambda \end{aligned} \quad (2.25)$$

The α and α' are Dirac indices, s is a 2-component spin index, summation over repeated indices is implied, and

$$\bar{\psi}_{s\alpha}^\nu \equiv \psi_{s\alpha}^{\dagger\nu}, \gamma_{\alpha'\alpha}^0 \quad (2.26)$$

We shall now write each deuteron wavefunction as a rest frame wavefunction boosted to the Breit frame. Our notation now will be that p is the spectator momentum in the Breit frame, p_1 is the spectator momentum when viewed in the rest frame of the initial deuteron, and p_2 will be the same momentum in the rest frame of the final deuteron. In the rest frames, the 3-vector part of the spectator momentum is the same as the 3-vector part of the relative momentum that we used in defining the wavefunctions u , w , v_t and v_s .

The Lorentz transformation properties of the $\psi_{s\alpha}^{\mu}$ are evident from its structure. First we note that any spinor is given by

$$u(\vec{p}, s) = S(L_p) u(\vec{0}, s) \quad (2.27)$$

where L_p is a boost in the \vec{p} direction, and that

$$S(L_p) = e^{\vec{\alpha} \cdot \hat{p} \xi/2}$$

$$\cosh \xi = E_p/M \quad (2.28)$$

and $\vec{\alpha}$ are the Dirac matrices (not to be confused with the index α).

Then for any boost Λ_1 in the z direction

$$S(\Lambda_1) u(\Lambda_1^{-1} \vec{p}, s) = u(\vec{p}, s') \mathcal{D}_{s's}^{(1/2)} (R_1)$$

$$S^{-1}(\Lambda_1) u^{-T}(\Lambda_1^{-1} \vec{p}, s) = u^{-T}(\vec{p}, s') \mathcal{D}_{s's}^{(1/2)*} (R_1) \quad (2.29)$$

where R_1 is the Wigner rotation

$$R_1 = L_p^{-1} \Lambda_1 L_{\Lambda_1^{-1} p} \quad (2.30)$$

Therefore the wavefunction in the moving frame is

$$\xi_\lambda \psi_{s\alpha}^\lambda(p, D) = \sqrt{\frac{M_d}{D_0}} s_{\alpha\alpha}, (\Lambda_1) \xi_{0\lambda} \psi_{s',\alpha}^\lambda(p_1, M_d) \mathcal{D}_{ss'}^{(1/2)}(R_1) \quad (2.31)$$

where ξ_0^λ are the polarization vectors (2.8) of the deuteron in its rest frame, and Λ_1 is now the boost from the rest frame of the initial deuteron to the Breit frame,

$$\begin{aligned} \Lambda_1 M_d &= D \\ \Lambda_1 p_1 &= p \\ \Lambda_1 \xi_0 &= \xi \end{aligned} \quad . \quad (2.32)$$

We now use (2.31) to replace the wavefunctions in (2.25) with rest system wavefunctions. We obtain

$$\begin{aligned} G^\mu(q^2) &= 2M_d \int d^3 p \frac{M}{E_p} \mathcal{D}_{ss_2}^{(1/2)*}(R_2) \xi_{0v}^{*\dagger} \bar{\psi}_{s_2\alpha}^v(p_2, M_d) \\ &\times \tilde{F}_{\alpha\alpha}^\mu, \xi_{0\lambda} \psi_{s_1\alpha}^\lambda(p_1, M_d) \mathcal{D}_{ss_1}^{(1/2)}(R_1) \end{aligned} \quad (2.33)$$

where the transformed form factor \tilde{F} is

$$\tilde{F}^\mu = S^{-1}(\Lambda_2) F^\mu S(\Lambda_1) \quad (2.34)$$

and Λ_2 and R_2 are the boost and Wigner rotation for the outgoing deuteron

$$\begin{aligned} \Lambda_2 M_d &= D' \\ \Lambda_2 &= \Lambda_1^{-1} \end{aligned} \quad . \quad (2.35)$$

Substituting the decomposition of the wavefunction into ψ^\pm into our formulae and remembering that summation over repeated indices is

implied gives us the result

$$\begin{aligned}
 G^\mu(q^2) = & 2M_d \int d^3p \left\{ \psi_{r_2 s_2}^{+\dagger}(\vec{p}_2) \tilde{F}_{r_2 r_1}^{\mu++} \psi_{s_1 r_1}^+(\vec{p}_1) \right. \\
 & + \psi_{r_2 s_2}^{+\dagger}(\vec{p}_2) \tilde{F}_{r_2 r_1}^{\mu+-} \psi_{s_1 r_1}^-(\vec{p}_1) \\
 & + \psi_{r_2 s_2}^{-\dagger}(\vec{p}_2) \tilde{F}_{r_2 r_1}^{\mu-+} \psi_{s_1 r_1}^+(\vec{p}_1) \\
 & \left. + \psi_{r_2 s_2}^{-\dagger}(\vec{p}_2) \tilde{F}_{r_2 r_1}^{\mu--} \psi_{s_1 r_1}^-(\vec{p}_1) \right\} \mathcal{D}_{s_2 s_1}^{(1/2)}(R_2^{-1} R_1) \quad (2.36)
 \end{aligned}$$

where the current matrix elements are

$$\begin{aligned}
 \tilde{F}_{r_2 r_1}^{\mu++} &= \frac{M}{E_p} \bar{u}(-\vec{p}_2, r_2) \tilde{F}^\mu u(-\vec{p}_1, r_1) \\
 \tilde{F}_{r_2 r_1}^{\mu-+} &= \frac{M}{E_p} \bar{v}(\vec{p}_2, -r_2) \tilde{F}^\mu u(-\vec{p}_1, r_1) \\
 \tilde{F}_{r_2 r_1}^{\mu+-} &= \frac{M}{E_p} \bar{u}(-\vec{p}_2, r_2) \tilde{F}^\mu v(\vec{p}_1, -r_1) \\
 \tilde{F}_{r_2 r_1}^{\mu--} &= \frac{M}{E_p} \bar{v}(\vec{p}_2, -r_2) \tilde{F}^\mu v(\vec{p}_1, -r_1) \quad (2.37)
 \end{aligned}$$

Equation (2.36) has a structure which can be easily understood.

It gives the form factor as a sum of 3 types of terms

$$G_\mu(q^2) = G_\mu^{++}(q^2) + G_\mu^{+-}(q^2) + G_\mu^{--}(q^2) , \quad (2.38)$$

where the first term, the $(++)$ term, corresponds to the virtual nucleon being in a positive energy state both before and after the interaction and is the relativistic generalization of the usual nonrelativistic impulse approximation. If the P-states of the deuteron were negligibly

small, this would be the only term which would contribute. The next term in (2.38), the (+-) term, corresponds to the overlap between positive and negative energy states. Finally, the last term gives the contribution from products of negative energy states alone.

The Wigner rotations $R_{1,2}$ are

$$\mathcal{D}^{(1/2)}(R_{1,2}) = e^{-\frac{1}{2}\sigma_3\phi} e^{-\frac{1}{2}\sigma_2\omega_{1,2}} e^{\frac{1}{2}\sigma_3\phi} \quad (2.39)$$

where ϕ is the azimuthal angle of \vec{p} and

$$\begin{aligned} \cos\left(\frac{1}{2}\omega_1\right) &= \frac{(E_p + M)(D_0 + M_d) - \frac{1}{2}p_z Q}{\sqrt{2M_d(E_1 + M)(E_p + M)(D_0 + M_d)}} \\ \sin\left(\frac{1}{2}\omega_1\right) &= \frac{\frac{1}{2}p_{\perp} Q}{\sqrt{2M_d(E_1 + M)(E_p + M)(D_0 + M_d)}} \end{aligned} \quad (2.40)$$

In these formulae, $p_z = p \cos \theta$, $p_{\perp} = p \sin \theta$, and $E_1 = (M^2 + \vec{p}_1^2)^{1/2}$.

The rotation R_2 has the same form, but with E_1 replaced by $E_2 = (M^2 + \vec{p}_2^2)^{1/2}$ in the denominator and Q replaced by $-Q$ in both numerators.

When these results are combined we obtain

$$\mathcal{D}^{(1/2)}(R_2^{-1}R_1) = \frac{\mathcal{M}_p + i\vec{\sigma} \cdot (\vec{p} \times \vec{Q}/2)}{M_d \sqrt{(E_1 + M)(E_2 + M)}} \quad (2.41)$$

where

$$\mathcal{M}_p = M_d E_p + D_0 M \quad . \quad (2.42)$$

C. The matrix elements of the current

The matrix elements of the current are straightforward, but tedious to calculate. We will merely list the results here, which can be expressed as matrices in a 2×2 spin space.

To calculate the charge and quadrupole form factors we need only the time component of the current, F^0 . Each of these matrices can be given in terms of two scalar functions:

$$\begin{aligned} \frac{2E_p}{\sqrt{(E_1 + M)(E_2 + M)}} \tilde{F}^{0++} &= X^{++} + i\vec{\sigma} \cdot (\vec{p} \times \vec{Q}) Y^{++} \\ \frac{2E_p}{\sqrt{(E_1 + M)(E_2 + M)}} \tilde{F}^{0+-} &= \vec{\sigma} \cdot \vec{Q} \left[X^{+-} + i\vec{\sigma} \cdot (\vec{p} \times \vec{Q}) \right] Y^{+-} . \quad (2.43) \end{aligned}$$

The expression for \tilde{F}^{0--} has the same form as that for \tilde{F}^{0++} , and $\tilde{F}^{0-+} = (\tilde{F}^{0+-})^\dagger$.

The X's and Y's are given in the formulae below, where $Q = |\vec{Q}|$ and $p_z = p \cos \theta$, $p_\perp = p \sin \theta$ and $K = M_d(E_1 + M)(E_2 + M)$.

$$KX^{++} = F_1 \frac{2E_p}{M} \mathcal{M}_p - \frac{Q^2}{2M} F_2 \left(\frac{2MD_0}{M_d^2} \mathcal{M}_p + \frac{p_\perp^2 Q^2}{2M_d^2} + p_\perp^2 \right)$$

$$KY^{++} = F_1 \frac{E_p}{M} + \frac{F_2}{M} \left(\mathcal{M}_p + \frac{Q^2}{2M_d} E_p \right)$$

$$\begin{aligned} KX^{+-} &= F_1 \left(\mathcal{M}_p \frac{M}{M_d} + D_0 \frac{p_\perp^2}{M_d} \right) \\ &+ F_2 \left[\frac{D_0}{M} \left(M^2 + p_z^2 + \frac{E_p D_0 M}{M_d} \right) - \frac{Q p_z \mathcal{M}_p}{2M M_d} \right] \end{aligned}$$

$$\begin{aligned}
 KY^{+-} &= F_1 \frac{p_z}{Q} + F_2 \left(\frac{1}{2} - \frac{D_0}{M_d M Q} (D_0 p_z - \frac{1}{2} Q E_p) \right) \\
 KX^{--} &= F_1 2E_p \mathcal{M}_p - \frac{F_2}{2M} Q^2 p_{\perp}^2 \\
 KY^{--} &= F_1 E_p + \frac{F_2}{M} \mathcal{M}_p
 \end{aligned} \tag{2.44}$$

To calculate the magnetic form factors we need the spatial components of the current. We calculate the (+) component defined as

$$\tilde{F}^{(+)} = \frac{1}{\sqrt{2}} \left[\tilde{F}^{(x)} + i \tilde{F}^{(y)} \right] \tag{2.45}$$

For these components it is convenient to introduce four scalar functions to describe our results:

$$\begin{aligned}
 \frac{2E_p}{\sqrt{(E_1 + M)(E_2 + M)}} \tilde{F}^{(+)++} &= Q X^{++} \sigma^+ + \frac{Y^{++}}{2p^-} + \frac{Z^{++}}{2p^-} \vec{\sigma} \cdot \vec{Q} + \frac{A^{++}}{p^-} Q \vec{\sigma} \cdot \vec{p}_{\perp} \\
 \frac{2E_p}{\sqrt{(E_1 + M)(E_2 + M)}} \tilde{F}^{(+)+-} &= X^{+-} \sigma^+ + \frac{Y^{+-}}{2p^-} + \frac{Z^{+-}}{2p^-} \sigma_3 + \frac{A^{+-}}{p^-} \vec{\sigma} \cdot \vec{p}_{\perp}
 \end{aligned} \tag{2.46}$$

where $p^- = \frac{1}{\sqrt{2}} (p_x - i p_y)$ and $\vec{p}_{\perp} = (p_x, p_y, 0)$. The decomposition for the (--) components is the same as for the (++) components, and the decomposition for the (-+) components is the same as the (+-). The functions are:

$$KX^{++} = F_1 \left[\frac{2D_0^2}{M_d^2} (M^2 + p_\perp^2) + \frac{2D_0 E_p M}{M_d} - p_\perp^2 \right] + \frac{F_2 E_p \mathcal{M}_p}{M}$$

$$KY^{++} = -F_1 p_\perp^2 \left[\frac{2E_p}{M_d} \left(D_0^2 + \frac{Q^2}{4} \right) + 2D_0 M \right] + \frac{F_2}{2M} E_p p_\perp^2 Q^2$$

$$KZ^{++} = F_1 2p_\perp^2 \frac{p_z D_0}{M_d} - F_2 \frac{D_0}{M} p_z p_\perp^2$$

$$KA^{++} = F_1 \frac{p_\perp^2}{2} - \frac{F_2}{2M} p_\perp^2 M_d$$

$$KX^{+-} = F_1 \left[\frac{-Q p_z}{M_d} + \frac{2D_0 E_p}{M_d} \right] \mathcal{M}_p$$

$$+ \frac{F_2 Q^2}{2M M_d} \left[D_0 p_z^2 - E_p (D_0 E_p + M M_d) \right]$$

$$KY^{+-} = F_1 \frac{Q p_\perp^2}{M_d} \left[-\frac{1}{2} Q p_z + D_0 E_p \right] + \frac{F_2}{M} Q p_\perp^2 \left[D_0 E_p + M M_d \right]$$

$$KZ^{+-} = F_1 \frac{p_\perp^2}{M_d} \left[Q (D_0 E_p + M_d M) - 2D_0^2 p_z \right] - \frac{F_2}{2M} Q^2 p_\perp^2 p_z$$

$$KA^{+-} = -F_1 D_0 p_\perp^2$$

$$KX^{--} = -F_1 p_\perp^2 - \frac{F_2}{M} E_p \mathcal{M}_p$$

$$KY^{--} = F_1 2p_\perp^2 \mathcal{M}_p - \frac{F_2}{2M} Q^2 p_\perp^2 E_p$$

$$KZ^{--} = F_2 \frac{D_0}{M} p_z p_\perp^2$$

$$KA^{--} = \frac{1}{2} F_1 p_\perp^2 + \frac{1}{2} \frac{F_2}{M} p_\perp^2 M_d$$

$$\begin{aligned} x^{-+}(p) &= x^{+-}(p) ; \quad y^{-+}(p) = y^{+-}(-p) \\ z^{-+}(p) &= -z^{+-}(-p) ; \quad a^{-+}(p) = a^{+-}(-p) . \end{aligned} \quad (2.47)$$

It is now a straightforward matter to combine these matrix elements with the Wigner rotations and the expressions giving ψ^\pm in terms of u , w , v_t and v_s . Since the indices for the wavefunctions in matrix form [Eq. (2.17)] are reversed, the expressions in (2.36) become a trace of products of Pauli matrices which are not difficult to evaluate. The terms in G_C and G_Q can be separated by averaging over ϕ . The results are given in the following section.

D. The final formulae

In this section we quote the final formulae. Each of the form factors can be written as a sum of three terms

$$G_i = G_i^{++} + G_i^{+-} + G_i^{--} \quad (2.48)$$

where $i = C, Q$, or M for the three form factors. Letting j stand for $(++)$, or $(+-)$, or $(--)$, we denote the typical term by G_i^j .

The G_i^j 's must be computed numerically by double integration over products of the momentum space wavefunctions:

$$G_i^j = \int_0^\infty p^2 dp \int_{-1}^{+1} dz \frac{1}{8D_0 E_p} \mathcal{J}_i^j . \quad (2.49)$$

Using the notation

$$u_{1,2} = u(p_{1,2}) - \frac{1}{\sqrt{2}} w(p_{1,2})$$

$$w_{1,2} = \frac{3}{\sqrt{2}} w(p_{1,2})$$

$$\begin{aligned}
 v_{1,2}^t &= -\sqrt{\frac{3}{2}} v_t(p_{1,2}) \\
 v_{1,2}^s &= \sqrt{3} v_s(p_{1,2}) \tag{2.50}
 \end{aligned}$$

the \mathcal{J} 's are:

$$\begin{aligned}
 \mathcal{J}_C^{++} &= (2\mathcal{M}_p X^{++} - p_{\perp}^2 Q^2 Y^{++}) \left[U_1 U_2 + \frac{2}{3} U_1 W_2 + \frac{1}{3} \frac{W_1 W_2}{p_1^2 p_2^2} (\vec{p}_1 \cdot \vec{p}_2)^2 \right] \\
 &+ (X^{++} + 2\mathcal{M}_p Y^{++}) \frac{1}{3} \frac{W_1 W_2}{p_1^2 p_2^2} \frac{E_p}{M_d} p_{\perp}^2 Q^2 (\vec{p}_1 \cdot \vec{p}_2) \\
 &+ Y^{++} Q^2 p_{\perp}^2 \frac{2}{3} U_1 U_2 \\
 \mathcal{J}_Q^{++} &= \frac{2M_d^2}{Q^2} \left\{ (2\mathcal{M}_p X^{++} - p_{\perp}^2 Q^2 Y^{++}) \left[\frac{U_1 W_2}{p_2^2} (2p_{2z}^2 - p_{\perp}^2) \right. \right. \\
 &+ \left. \frac{W_1 W_2}{p_1^2 p_2^2} (\vec{p}_1 \cdot \vec{p}_2) (p_{1z} p_{2z} - \frac{1}{2} p_{\perp}^2) \right] \\
 &+ (X^{++} + 2\mathcal{M}_p Y^{++}) p_{\perp}^2 Q^2 \left[\frac{3U_1 W_2}{p_2^2} p_{2z} + \frac{W_1 W_2}{p_1^2 p_2^2} \frac{QE_p}{M_d} (p_{1z} p_{2z} - \frac{1}{2} p_{\perp}^2) \right] \\
 &\left. - Y^{++} p_{\perp}^2 Q^2 U_1 U_2 \right\} \\
 \mathcal{J}_M^{++} &= 2M_d \left\{ (U_1 U_2 + U_1 W_2) \left[2\mathcal{M}_p (X^{++} + A^{++}) - \frac{1}{2} (Y^{++} - QZ^{++}) \right] \right. \\
 &+ \frac{U_1 W_2}{p_2^2} \left[-(X^{++} + 2A^{++}) p_{\perp}^2 (\mathcal{M}_p - \frac{Q}{2} p_{2z}) - Z^{++} (\mathcal{M}_p p_{2z} + \frac{Q}{2} p_{\perp}^2) \right] \\
 &\left. + \frac{W_1 W_2}{p_1^2 p_2^2} \left[X^{++} p_{\perp}^2 Q^2 \left(\frac{\mathcal{M}_p E_p^2}{2M_d^2} - \frac{E_p}{4M_d} (\vec{p}_1 \cdot \vec{p}_2) \right) \right. \right.
 \end{aligned}$$

$$- Y^{++} \left(\mathcal{M}_p (\vec{p}_1 \cdot \vec{p}_2) \frac{E_p}{2M_d} + \frac{p_\perp^2 Q^2 E_p^2}{4M_d^2} \right) \right] \Big\}$$

$$\begin{aligned}
 \mathcal{I}_C^{+-} &= 2(2\mathcal{M}_p^{X^{+-}} + p_\perp^2 Q^2 Y^{+-}) \left[\frac{2}{3} U_2 \frac{V_1^t}{p_1} p_{1z} Q + \frac{1}{3} U_2 \frac{V_1^s}{p_1} p_{1z} Q \right. \\
 &+ \frac{1}{3} \frac{W_2 V_1^t}{p_2^2 p_1} Q^2 p_\perp^2 \frac{E_p}{M_d} + \frac{1}{3} \frac{W_2 V_1^s}{p_2^2 p_1} Q p_{2z} (\vec{p}_1 \cdot \vec{p}_2) \Big] \\
 &+ 2(X^{+-} - 2\mathcal{M}_p^{Y^{+-}}) \frac{p_\perp^2 Q^2}{3} \left[\frac{U_2 V_1^s}{p_1} - \frac{W_2 V_1^t}{p_2^2 p_1} \frac{p_{2z}}{M_d} Q E_p + \frac{W_2 V_1^s}{p_2^2 p_1} (\vec{p}_1 \cdot \vec{p}_2) \right] \\
 &- 2Y^{+-} p_\perp^2 Q^2 \frac{2}{3} \frac{U_2 V_1^t}{p_1} (2\mathcal{M}_p + Q p_{1z}) \\
 \mathcal{I}_Q^{+-} &= 4M_d^2 \left\{ (2\mathcal{M}_p^{X^{+-}} + p_\perp^2 Q^2 Y^{+-}) \left[\frac{-U_2 V_1^t}{p_1} \frac{p_{1z}}{Q} + \frac{U_2 V_1^s}{p_1} \frac{p_{1z}}{Q} \right. \right. \\
 &- \frac{W_2 V_1^t}{p_2^2 p_1} \frac{p_\perp^2}{Q} (p_{2z} + \frac{1}{2} p_{1z}) + \frac{W_2 V_1^s}{p_2^2 p_1} \frac{p_{2z}}{Q} (p_{1z} p_{2z} - \frac{1}{2} p_\perp^2) \Big] \\
 &+ (X^{+-} - 2\mathcal{M}_p^{Y^{+-}}) p_\perp^2 \left[\frac{3}{2} \frac{U_2 V_1^t}{p_1} - \frac{1}{2} \frac{U_2 V_1^s}{p_1} \right. \\
 &+ \frac{W_2 V_1^t}{p_2^2 p_1} p_{2z} (p_{2z} + \frac{1}{2} p_{1z}) + \frac{W_2 V_1^s}{p_2^2 p_1} (p_{1z} p_{2z} - \frac{1}{2} p_\perp^2) \Big] \\
 &+ Y^{+-} p_\perp^2 \frac{U_2 V_1^t}{p_1} (2\mathcal{M}_p + Q p_{1z}) \Big\}
 \end{aligned}$$

$$\begin{aligned}
 \mathcal{I}_M^{+-} &= \frac{2M_d}{Q} \left\{ U_2 \left(\frac{v_1^s}{p_1} + \frac{v_1^t}{p_1} \right) \left[-X^{+-} (2p_{1z} \mathcal{M}_p + \frac{1}{2} Q p_\perp^2) \right. \right. \\
 &+ Y^{+-} \mathcal{M}_p + Z^{+-} (\mathcal{M}_p - \frac{1}{2} Q p_{1z}) - A^{+-} Q p_\perp^2 \left. \right] \\
 &+ U_2 \left(\frac{v_1^s}{p_1} - \frac{v_1^t}{p_1} \right) \left[-Y^{+-} (\mathcal{M}_p + \frac{1}{2} Q p_{1z}) - A^{+-} 2p_{1z} \mathcal{M}_p \right] \\
 &+ \frac{v_1^s w_2}{p_1 p_2^2} \left[-(X^{+-} + 2A^{+-}) \frac{p_\perp^2 Q E_p}{M_d} (\mathcal{M}_p - \frac{1}{2} p_{2z} Q) \right. \\
 &- \frac{Z^{+-} Q E_p}{M_d} (\mathcal{M}_p p_{2z} + \frac{1}{2} Q p_\perp^2) \left. \right] \\
 &+ \frac{v_1^t w_2}{p_1 p_2^2} \left[X^{+-} \left(-2(\vec{p}_1 \cdot \vec{p}_2) (\mathcal{M}_p p_{2z} + \frac{1}{4} Q p_\perp^2) - \frac{Q^2 p_\perp^2 p_{2z} E_p}{2M_d} \right) \right. \\
 &+ Y^{+-} p_{2z} \left(-\frac{\mathcal{M}_p Q E_p}{M_d} + \frac{1}{2} Q (\vec{p}_1 \cdot \vec{p}_2) \right) + Z^{+-} (\vec{p}_1 \cdot \vec{p}_2) (\mathcal{M}_p - \frac{1}{2} Q p_{2z}) \\
 &+ A^{+-} (p_{1z} p_{2z} - p_\perp^2) (2\mathcal{M}_p p_{2z} + Q p_\perp^2) \left. \right] \} \\
 \mathcal{I}_C^{--} &= 2\mathcal{M}_p^{X^{--}} \frac{2}{3} \frac{v_1^t v_2^t}{p_1 p_2} (\vec{p}_1 \cdot \vec{p}_2) \\
 &+ (2\mathcal{M}_p^{Y^{--}} + X^{--}) \frac{1}{3} \frac{v_1^t v_2^t}{p_1 p_2} p_\perp^2 Q^2 \frac{E_p}{M_d} \\
 &+ (2\mathcal{M}_p^{X^{--}} + p_\perp^2 Q Y^{--}) \frac{1}{3} \frac{v_1^s v_2^s}{p_1 p_2} (\vec{p}_1 \cdot \vec{p}_2) \\
 &+ (2\mathcal{M}_p^{Y^{--}} - X^{--}) \frac{2}{3} p_\perp^2 Q^2 \frac{E_p}{M_d} \frac{v_2^s v_1^t}{p_1 p_2}
 \end{aligned}$$

$$\begin{aligned}
 \mathcal{I}_Q^{--} &= 2M_d^2 \left\{ \frac{2\mathcal{M}_p X^{--}}{Q^2} \frac{v_{12}^t v_{12}^t}{p_1 p_2} \left(\frac{1}{2} p_\perp^2 - p_{1z} p_{2z} \right) \right. \\
 &+ Y^{--} \frac{v_{12}^t v_{12}^t}{p_1 p_2} \frac{3}{2} p_\perp^4 - (2\mathcal{M}_p Y^{--} + X^{--}) \frac{v_{12}^t v_{12}^t}{p_1 p_2} \frac{p_\perp^2 E_p}{2M_d} \\
 &+ (2\mathcal{M}_p X^{--} + p_\perp^2 Q^2 Y^{--}) \frac{v_{12}^s v_{12}^s}{p_1 p_2} \frac{(p_{1z} p_{2z} - \frac{1}{2} p_\perp^2)}{Q^2} \\
 &\left. + 2(2\mathcal{M}_p Y^{--} - X^{--}) \frac{p_\perp^2}{Q} \frac{v_{12}^t v_{12}^s}{p_1 p_2} (p_{1z} + \frac{1}{2} p_{2z}) \right\} \\
 \mathcal{I}_M^{--} &= 2M_d \left\{ \frac{v_{12}^t v_{12}^t}{p_1 p_2} \left[X^{--} p_\perp^2 (\mathcal{M}_p + Q p_{1z}) - \frac{Y^{--} \mathcal{M}_p p_{1z}}{Q} \right. \right. \\
 &+ Z^{--} (p_{1z} \mathcal{M}_p - \frac{1}{2} Q p_\perp^2) + A^{--} p_\perp^2 (2\mathcal{M}_p + Q p_{1z}) \left. \right] \\
 &+ \frac{v_{12}^s v_{12}^s}{p_1 p_2} \left[-X^{--} \frac{1}{2} Q p_\perp^2 p_{2z} + \frac{Y^{--} \mathcal{M}_p p_{2z}}{Q} \right] \\
 &+ \frac{v_{12}^t v_{12}^s}{p_1 p_2} \left[-X^{--} \mathcal{M}_p (\vec{p}_1 \cdot \vec{p}_2) - (X^{--} + 2A^{--}) p_{2z} (\mathcal{M}_p p_{1z} - \frac{1}{2} Q p_\perp^2) \right. \\
 &\left. \left. - Y^{--} \frac{1}{2} (\vec{p}_1 \cdot \vec{p}_2) + Z^{--} p_{2z} (\mathcal{M}_p + \frac{1}{2} Q p_{1z}) \right] \right\} \quad (2.51)
 \end{aligned}$$

Recall that \vec{p}_1 and \vec{p}_2 are the relative 3-momentum of the incoming and outgoing deuteron, respectively. We have

$$\vec{p}_{1,2} = \left(p_\perp, \frac{D_0 p_z \pm \frac{1}{2} Q E_p}{M_d} \right) = (p_\perp, p_{1z}, p_{2z}) \quad (2.52)$$

E. The ultrahigh Q^2 limit

The ultrahigh Q^2 limit means that $Q^2 \gg 4M_d^2$. This is beyond the range of current experiment, but asymptotic formulae are of particular interest as discussed in Section I.

As a first step toward determining the power dependence of the form factors on Q^2 in the ultrahigh Q^2 region, we study the generic overlap integral

$$I(Q) = \int d^3p \ u(p_1) u'(p_2) \quad (2.53)$$

where u and u' stand for any one of the four deuteron wavefunctions, and p_1 and p_2 are the magnitudes of the Lorentz transformed 3-momenta given in (2.52), i.e., the magnitudes of the internal relative momenta of the incoming and outgoing deuterons evaluated in their respective rest frames. We will assume that

$$u(p) \xrightarrow[p \rightarrow \infty]{} p^{-N} \quad (2.54)$$

In order to discuss this integral in a reasonably general way, we assume that each of the four wavefunctions has a momentum space expansion of the form

$$u(p) = \sum_i \frac{c_i}{p^2 + \beta_i^2} \quad (2.55)$$

which corresponds to a position space expansion in Hulthen functions of different range

$$\frac{u(r)}{r} = \sqrt{\frac{\pi}{2}} \sum_i c_i \frac{e^{-\beta_i r}}{r} \quad (2.56)$$

If we define the n th moment of the coefficients as

$$M_n = \sum_i c_i \beta_i^n \quad (2.57)$$

then when the first n moments of the coefficients are zero, the reduced wavefunction $u(r)$ will go like r^{n-1} at the origin, and the momentum space wavefunction will go like $p^{-(n+2)}$ if n is even and $p^{-(n+1)}$ if n is odd.

The problem has, therefore, been reduced to understanding the behavior of the typical integral

$$I_{ij}(Q) = \int d^3 p \frac{1}{(p_1^2 + \beta_i^2)(p_2^2 + \beta_j^2)} \quad (2.58)$$

where, from (2.52)

$$p_{1,2}^2 = p_\perp^2 + \frac{1}{M_d^2} (D_0 p_z \pm \frac{1}{2} Q E_p)^2 \quad (2.59)$$

For comparison, the corresponding momenta in the non-relativistic case are simply

$$p_\pm^2 = p_\perp^2 + (p_z \pm \frac{1}{2} Q)^2 \quad (2.60)$$

The integral (2.58) can be evaluated exactly by first integrating over p_z in the complex p_z plane and then doing the p_\perp integration by standard means. The result is

$$I_{ij} = \frac{2\pi^2 M_d^3}{Q M D_0^2} \left\{ \frac{(\gamma_i + \gamma_j)M}{2\gamma_i \gamma_j} \left(\frac{\pi}{2} - \arctan \left[\frac{\beta_i + \beta_j}{\gamma_i + \gamma_j} \frac{2D_0}{Q} \right] \right) \right. \\ \left. - \frac{|\gamma_i - \gamma_j| M}{2\gamma_i \gamma_j} \left(\frac{\pi}{2} - \arctan \left[\frac{\beta_i + \beta_j}{|\gamma_i - \gamma_j|} \frac{2D_0}{Q} \right] \right) \right\} \quad (2.61)$$

where

$$\gamma_i = \sqrt{M^2 - \beta_i^2} \quad (2.62)$$

It is then a straightforward matter to expand this result in a power series in Q^{-1} , and obtain the results quoted in Ref. 2.

However, it is useful for our purposes to discuss the behavior of (2.58) from another point of view. From (2.59) we see that the minimum value of p_1^2 (or p_2^2) occurs when

$$\begin{aligned} p_{\perp} &= 0 \\ p_z &= \pm \frac{Q}{2M_d} \sqrt{M^2 + p_{\perp}^2} = \pm \frac{QM}{2M_d} \end{aligned} \quad (2.63)$$

At these two points, which we shall refer to as the "end points," one wavefunction has $p^2 = 0$ and the other wavefunction has

$$p^2 \underset{Q \rightarrow \infty}{\simeq} \frac{Q^4 M^2}{4M_d^4} \quad (2.64)$$

One might expect that the integral would be dominated by contributions from the end points, as is the case non-relativistically. However, examination of the full denominator in (2.58) shows that, as $Q \rightarrow \infty$ the denominator is of order Q^4 over the entire region defined by

$$\begin{aligned} p_{\perp} &\lesssim M \\ p_z &\lesssim Q \end{aligned} \quad (2.65)$$

so that the end points are not specifically favored. (Non-relativistically, the denominator is of order Q^4 everywhere, except at the end points where it is of order Q^2 .) Away from the end points, the Q^4 behavior comes from a Q^2 behavior from each wavefunction, which means

that the momentum of each wavefunction is large. Hence, we conclude that the original integral (2.53) goes at ultrahigh momentum transfer like

$$I(Q) \rightarrow Q^{-(2N-1)} \quad (2.66)$$

where the extra power of Q comes from the volume of the region (2.65). (This can be obtained by expanding (2.61).)

Finally, we turn to the question of how the form factors themselves behave at ultrahigh Q^2 . Since the wavefunctions do not peak in any well defined region, the behavior of the kinematic factors will determine what region of the p_z, p_\perp space dominates the integrand. For example, if an extra factor of p_z can be found in the numerator, it must be assumed to be of the order Q , and the integrand is dominated by the end points, whereas a factor of p_z in the denominator will tend to restrict the integrand to small values of $p_z \lesssim M$. Note, however, that a single power of p_z in the denominator will contribute a factor of

$$p_z^{-1} \xrightarrow[Q \rightarrow \infty]{} Q^{-1} \ln Q \quad (2.67)$$

since the integrand will reach large Q before convergence is imposed by the wavefunction.

Finally, when the kinematic factors are thoroughly examined, we obtain the following results:

$$\begin{aligned} G_C &\xrightarrow[Q \rightarrow \infty]{} Q^{-(2N+4)} \ln Q \\ G_Q &\xrightarrow{} Q^{-(2N+6)} \ln Q \\ G_M &\xrightarrow{} Q^{-(2N+4)} \ln Q \end{aligned} \quad (2.68)$$

where we have assumed a Q^{-4} falloff for the nucleon electromagnetic form factors.

The behavior of the A and B form factors follows from Eq. (1.4), and ignoring the $\log Q$ terms we obtain the results given in Eq. (1.9). The final results depend on N, as discussed in Section I-D.

We turn now to a discussion of our low Q^2 results.

F. The formulae for low Q^2

Formulae for low Q^2 have been obtained previously, and so we shall take the low Q^2 limit of our formulae mainly to show our agreement with the earlier work. By low Q^2 we mean that $\eta = Q^2/4M_d^2 \ll 1$, so it is only necessary to retain terms of first order in $(Q/M)^2$. However, we will not assume Q^2 is so small that it is much less than \vec{p}^2 , a typical value of the integration variable. Assuming that the dominant contributions come from the (++) parts, we will calculate these to first order in $(Q/M)^2$, and the remainder only to lowest-order. Furthermore, we will calculate the magnetic form factor only to lowest-order, since the leading contribution from this term to $A(Q^2)$ is only of order η anyway.

With these simplifications, the momentum space formulae can be written (following the standard style for low Q^2 results)

$$\begin{aligned} G_C &= G_{ES} D_C + (2G_{MS} - G_{ES}) D_C^{SO} \\ G_Q &= G_{ES} D_Q + (2G_{MS} - G_{ES}) D_Q^{SO} \\ G_M &= G_{ES} D_M^E + G_{MS} D_M^M \end{aligned} \tag{2.69}$$

where G_{ES} and G_{MS} are the isoscalar electric and magnetic form factors of the nucleon, related to F_{1S} and F_{2S} by

$$G_{ES} = F_{1S} - \frac{Q^2}{4M^2} F_{2S} \quad (2.70)$$

$$G_{MS} = F_{1S} + F_{2S}$$

and the D's are body form factors involving the deuteron wavefunctions.

We have,

$$D_C = D_C^{++} + D_C^{--}$$

$$D_C^{SO} = D_C^{SO++} + D_C^{SO+-}$$

$$D_Q = D_Q^{++} + D_Q^{--}$$

$$D_Q^{SO} = D_Q^{SO++} + D_Q^{SO+-}$$

$$D_M^M = D_M^{M++} + D_M^{M--}$$

$$D_M^E = D_M^{E++} + D_M^{E+-} + D_M^{E--} \quad (2.71)$$

where

$$D_C^{++} = \frac{M_d}{D_0} \int \frac{d^3 p}{4\pi} \left[u_1 u_2 + w_1 w_2 \vec{p}_2 (\vec{p}_1 \cdot \vec{p}_2) \right]$$

$$D_C^{--} = \int \frac{d^3 p}{4\pi} \left[v_{t+} v_{t-} (\hat{p}_+ \cdot \hat{p}_-) + v_{s+} v_{s-} (\hat{p}_+ \cdot \hat{p}_-) \right]$$

$$D_C^{SO++} = \frac{3Q^2}{16M^2} \int \frac{d^3 p}{4\pi} \frac{w_+ w_-}{p_+^2 p_-^2} p_\perp^2 (\vec{p}_1 \cdot \vec{p}_2)$$

$$\begin{aligned}
 D_C^{so+-} &= \frac{Q}{2M} \int \frac{d^3 p}{4\pi} \left\{ -\sqrt{\frac{2}{3}} u_- v_{t+} (\hat{p}_+ \cdot \hat{Q}) + \frac{1}{\sqrt{3}} u_- v_{s+} (\hat{p}_+ \cdot \hat{Q}) \right. \\
 &+ \left. \sqrt{\frac{3}{2}} w_- \left(\frac{v_{t+}}{\sqrt{2}} + v_{s+} \right) \left[(\hat{p}_- \cdot \hat{Q}) (\hat{p}_- \cdot \hat{p}_+) - (\hat{p}_+ \cdot \hat{Q}) \frac{1}{3} \right] \right\} \\
 D_Q^{++} &= \frac{6\sqrt{2} M_d^2}{Q^2} \frac{M_d}{D_0} \int \frac{d^3 p}{4\pi} \left\{ u_2 w_1 p_2 (\hat{p}_1 \cdot \hat{Q}) \right. \\
 &+ \frac{w_1 w_2}{\sqrt{2}} \left[\frac{3}{2} (\hat{p}_1 \cdot \hat{p}_2) \left(\frac{3}{2} (\hat{p}_1 \cdot \hat{Q}) (\hat{p}_2 \cdot \hat{Q}) - \frac{1}{2} (\hat{p}_1 \cdot \hat{p}_2) \right) \right. \\
 &- \left. \left. p_2 (\hat{p}_1 \cdot \hat{Q}) \right] \right\} \\
 D_Q^{--} &= \frac{2M_d^2}{Q^2} \int \frac{d^3 p}{4\pi} \left[3v_{s+} v_{s-} - \frac{3}{2} v_{t+} v_{t-} \right] \\
 &\times \left[\frac{3}{2} (\hat{p}_+ \cdot \hat{Q}) (\hat{p}_- \cdot \hat{Q}) - \frac{1}{2} (\hat{p}_+ \cdot \hat{p}_-) \right] \\
 D_Q^{so++} &= \frac{6\sqrt{2} M_d^2}{Q^2} \frac{1}{4M^2} \int \frac{d^3 p}{4\pi} \left\{ \frac{u_+ w_-}{p_-^2} - \frac{3}{2} p_\perp^2 (\vec{Q} \cdot \vec{p}_-) \right. \\
 &+ \frac{w_+ w_-}{\sqrt{2} p_+^2 p_-^2} \left[\frac{3p_\perp^2 Q^2}{4} \left(\frac{3}{2} (\vec{p}_+ \cdot \hat{Q}) (\vec{p}_- \cdot \hat{Q}) - \frac{1}{2} (\vec{p}_+ \cdot \vec{p}_-) \right) \right. \\
 &- \left. \left. \frac{3}{4} p_\perp^2 (\vec{p}_- \cdot \vec{Q}) p_+^2 \right] \right\} \\
 D_M^{M++} &= \int \frac{d^3 p}{4\pi} \left[2u_+ u_- + \sqrt{2} u_+ w_- p_2 (\hat{p}_- \cdot \hat{Q}) \right. \\
 &- \left. \frac{w_+ w_-}{2} \left(4p_2 (\hat{p}_+ \cdot \hat{Q}) p_2 (\hat{p}_- \cdot \hat{Q}) + 9p_\perp^2 \frac{(\vec{p}_+ \cdot \hat{Q}) (\vec{p}_- \cdot \hat{Q})}{p_+^2 p_-^2} \right) \right]
 \end{aligned}$$

$$\begin{aligned}
 D_M^{M--} &= \int \frac{d^3 p}{4\pi} \left[\frac{v_{t+} v_{t-}}{p_+ p_-} \left(-\frac{3}{2} p_\perp^2 \right) \right. \\
 &\quad \left. - \frac{3}{\sqrt{2}} \frac{v_{t+} v_{s-}}{p_+ p_-} (\vec{p}_+ \cdot \vec{p}_- + (\vec{p}_+ \cdot \hat{Q}) (\vec{p}_- \cdot \hat{Q})) \right] \\
 D_M^{E++} &= - \int \frac{d^3 p}{4\pi} \frac{w_s w_{-}}{p_+^2 p_-^2} \frac{9 p_\perp^2}{Q^2} (\vec{p}_- \cdot \vec{Q}) (\vec{p}_+ \cdot \vec{p}_-) \\
 D_M^{E+-} &= \frac{2M}{Q} \int \frac{d^3 p}{4\pi} \left[-2\sqrt{3} (\hat{p}_+ \cdot \hat{Q}) v_{s+} u_{-} + \sqrt{6} (\hat{p}_+ \cdot \hat{Q}) v_{t+} u_{-} \right. \\
 &\quad \left. + \frac{v_{s+} w_{-}}{p_-^2} \left(2\sqrt{\frac{3}{2}} p_-^2 (\vec{p}_+ \cdot \hat{Q}) - \frac{3}{2} \sqrt{\frac{3}{2}} Q p_\perp^2 \right) \right. \\
 &\quad \left. + \frac{v_{t+} w_{-}}{p_-^2} (3\sqrt{3} (\vec{p}_+ \cdot \vec{p}_-) (\vec{p}_- \cdot \hat{Q}) - \sqrt{3} p_-^2 (\vec{p}_+ \cdot \hat{Q})) \right] \\
 D_M^{E--} &= \int \frac{d^3 p}{4\pi} \left[\frac{3}{4} \frac{v_{t+} v_{t-}}{p_+ p_-} p_\perp^2 - \frac{3}{2} \frac{v_{s+} v_{s-}}{p_+ p_-} p_\perp^2 \right. \\
 &\quad \left. + \frac{3}{\sqrt{2}} \frac{v_{t+} v_{s-}}{p_+ p_-} (\vec{p}_+ \cdot \vec{p}_- + (\vec{p}_+ \cdot \hat{Q}) (\vec{p}_- \cdot \hat{Q})) \right] \quad (2.72)
 \end{aligned}$$

The arguments of the momentum space wavefunctions have been abbreviated 1, 2, +, or -, depending on whether they are p_1 , p_2 , p_+ , or p_- (cf. Eqs. (2.59) and (2.60)). P_2 is the Legendre polynomial.

As stated above, in the largest terms D_C^{++} and D_Q^{++} , we retain the integrands accurate to first-order in η . In this case, realizing that if $Q/M \ll 1$ then $p/M \ll 1$ also, we expand (2.59) to obtain

$$\vec{p}_{1,2} = \vec{p}_{\pm} + \vec{Q} \left(\frac{\vec{p} \cdot \vec{Q}}{32M^2} + \frac{p^2 + \alpha^2}{8M^2} \right)$$

$$p_{1,2} = |\vec{p}_{1,2}| \quad (2.73)$$

where $\alpha = M\epsilon$ and ϵ is the binding energy of the deuteron. In all cases \hat{x} represents a unit vector in the \hat{x} direction (for any x).

While the low Q^2 formulae (2.72) are simple enough, it is possible to reduce them to a single integral if we transform them to position space. (Unfortunately, this is not possible for the exact formulae (2.49).) To do so we use the identities

$$w(p) Y_{2M}(\hat{p}) = -\frac{1}{4\pi} \int d^3r e^{ip \cdot \vec{r}} Y_{2M}(\hat{r}) \frac{w(r)}{r}$$

$$u(p) Y_{00}(\hat{p}) = \frac{1}{4\pi} \int d^3r e^{ip \cdot \vec{r}} Y_{00}(\hat{r}) \frac{u(r)}{r}$$

$$v(p) Y_{1M}(\hat{p}) = -\frac{i}{4\pi} \int d^3r e^{ip \cdot \vec{r}} Y_{1M}(\hat{r}) \frac{v(r)}{r} \quad (2.74)$$

$$w(p) Y_{00}(\hat{p}) = -\frac{1}{4\pi} \int d^3r e^{ip \cdot \vec{r}} Y_{00}(\hat{r}) \left[\frac{w(r)}{r} + 3 \int_0^r dr' \frac{w(r')}{r'^2} \right]$$

All the angular functions in the formulae (2.72) can be expanded in Y_{lm} 's so that the only combinations needed are those given above in (2.74). It also turns out that terms involving the integral over w cancel. For the more complicated terms D_C^{++} and D_Q^{++} , we note that except for the factor M_d/D_0 all of the $(Q/M)^2$ terms come from the arguments p_1 and p_2 , and, using a Taylor expansion, we can express these terms as:

$$\int d^3 p \frac{M_d}{D_0} f(p_{1z}, p_{2z}, p_{\perp}) \quad (2.75a)$$

$$\cong \left(1 - \frac{Q^2}{32M^2} \right) \int d^3 p \left[1 + \frac{p_z Q^2}{32M^2} \frac{\partial}{\partial p_z} + \frac{p_z^2 + \alpha^2}{M^2} Q^2 \frac{\partial}{\partial Q^2} \right] f(p_{+z}, p_{-z}, p_{\perp})$$

$$\cong \left[1 - \frac{Q^2}{8M^2} - \frac{Q^4}{16M^2} \frac{\partial}{\partial Q^2} \right] \int d^3 p f(p_{+z}, p_{-z}, p_{\perp})$$

$$+ Q^2 \frac{\partial}{\partial Q^2} \int d^3 p \left[\frac{p_+^2 + \alpha^2}{2M^2} + \frac{p_-^2 + \alpha^2}{2M^2} \right] f(p_{+z}, p_{-z}, p_{\perp}) \quad (2.75b)$$

The last term on the RHS of (2.75b), with the Schrodinger operators $p_{\pm}^2 + \alpha^2$, gives rise to the "potential" corrections included by Coester and Ostebree²⁸ and also by Gross.²⁹ Only the first set of terms was obtained by Friar.¹² In order to remove the "potential" terms we would have to remove also the last term from the previous expression (2.75a), but we would then lose the other derivative term (obtained by Friar) in (2.75b). Hence, from the point of view of our calculation the "potential" terms are essentially interrelated with the other corrections.

Next, we give the position space form of these low Q^2 results. If $\tau = Qr/2$, and j_{ℓ} is the spherical Bessel function of order ℓ , then

$$D_C = \int_0^{\infty} dr j_0(\tau) [u^2 + w^2 + v_t^2 + v_s^2]$$

$$- \left(\frac{Q^2}{8M^2} + \frac{Q^4}{16M^2} \frac{d}{dQ^2} \right) \int_0^{\infty} dr j_0(\tau) (u^2 + w^2)$$

$$+ \frac{Q^2}{M^2} \frac{d^2}{dQ^2} \int_0^{\infty} dr j_0(\tau) \left[u \left(-\frac{d^2}{dr^2} + \alpha^2 \right) u + w \left(-\frac{d^2}{dr^2} + \frac{6}{r^2} + \alpha^2 \right) w \right]$$

$$\begin{aligned}
 D_C^{SO} &= \frac{Q^2}{12M^2} \int_0^\infty dr \left(j_0(\tau) + j_2(\tau) \right) \\
 &\times \left\{ \frac{3}{2} w^2 - Mr \sqrt{\frac{3}{2}} v_t (u + \frac{w}{2}) + \frac{Mr}{\sqrt{3}} v_s (u - \sqrt{2}w) \right\} \\
 \frac{Q^2}{6\sqrt{2} M_d^2} D_Q &= \int_0^\infty dr j_2(\tau) \left[uw - \frac{w^2}{2\sqrt{2}} + \frac{v_t^2}{2\sqrt{2}} - \frac{v_s^2}{\sqrt{2}} \right] \\
 &- \left(\frac{Q^2}{8M^2} + \frac{Q^4}{16M^2} \frac{d^2}{dQ^2} \right) \int_0^\infty dr j_2(\tau) \left[uw - \frac{w^2}{2\sqrt{2}} \right] \\
 &+ \frac{Q^2}{2M^2} \frac{d^2}{dQ^2} \int_0^\infty dr j_2(\tau) \left[w \left(-\frac{d^2}{dr^2} + \alpha^2 \right) u \right. \\
 &\left. + u \left(-\frac{d^2}{dr^2} + \frac{6}{r^2} + \alpha^2 \right) w - \frac{w}{\sqrt{2}} \left(-\frac{d^2}{dr^2} + \frac{6}{r^2} + \alpha^2 \right) w \right] \\
 D_Q^{SO} &= \int_0^\infty dr \left\{ \left[\sqrt{2} rwu' - \sqrt{2} wu - rww' \right] \right. \\
 &\times \left[\frac{3}{5} (j_0(\tau) + j_2(\tau)) + \frac{9}{35} (j_2(\tau) + j_4(\tau)) \right] \\
 &+ Mr \left[u \frac{\sqrt{3}}{2} v_t + u\sqrt{3} v_s \right] \frac{2}{3} (j_0(\tau) + j_2(\tau)) \\
 &- Mr (\sqrt{3} wv_t) \left[\frac{9}{35} (j_2(\tau) + j_4(\tau)) + \frac{4}{15} (j_0(\tau) + j_2(\tau)) \right] \\
 &\left. + Mr \left(\frac{\sqrt{3}}{2} wv_s \right) \left[\frac{18}{35} (j_2(\tau) + j_4(\tau)) - \frac{2}{15} (j_0(\tau) + j_2(\tau)) \right] \right\}
 \end{aligned}$$

$$\begin{aligned}
 D_M^M &= \int_0^\infty dr \left[(2u^2 - w^2 - v_t^2 - 2\sqrt{2} v_t v_s) j_0(\tau) \right. \\
 &\quad \left. + (\sqrt{2} uw + w^2 - v_t^2 + \sqrt{2} v_t v_s) j_2(\tau) \right] \\
 D_M^E &= \int_0^\infty dr \left[\left(\frac{3}{2} w^2 - v_s^2 + \frac{1}{2} v_t^2 \right) (j_0(\tau) + j_2(\tau)) \right. \\
 &\quad + \frac{2Mr}{\sqrt{3}} \left(v_t \left(\frac{1}{\sqrt{2}} u - w \right) - v_s \left(u + \frac{1}{\sqrt{2}} w \right) \right) (j_0(\tau) + j_2(\tau)) \\
 &\quad \left. + v_t v_s \sqrt{2} (2j_0(\tau) - j_2(\tau)) \right] \tag{2.76}
 \end{aligned}$$

Finally, we record here the additional contributions to the magnetic moment and quadrupole moment presented in Eqs. (1.15) and (1.16). They are written as integrals over the full momentum space wave functions and their derivatives (denoted by a prime).

$$\begin{aligned}
 \Delta_\mu &= \int_0^\infty p^2 dp \left\{ \frac{-(E-M)}{3\sqrt{2} E} \left[(u + \sqrt{2} w) (\sqrt{2} u - w) + \frac{\tilde{F}_2}{\sqrt{2}} (\sqrt{2} u - w)^2 - 3v_t^2 \right] \right. \\
 &\quad + \frac{1}{\sqrt{3}} (E - M) \left[- \frac{1}{\sqrt{2}} (\sqrt{2} u - w) (v_s' + \frac{v_s}{p}) + \frac{u}{5\sqrt{2}} (7v_t' + \frac{8v_t}{p}) \right. \\
 &\quad \left. + \frac{w}{35} (37v_t' - 16 \frac{v_t}{p}) \right] - \frac{1}{\sqrt{3}} \frac{p}{E} \tilde{F}_2 v_t (\sqrt{2} u - w) \\
 &\quad \left. + \frac{p^3}{\sqrt{3} E (E+M)^2} \left(- \frac{1}{5\sqrt{2}} uv_t + \frac{1}{7} wv_t \right) \right\}
 \end{aligned}$$

$$\begin{aligned}
 \Delta_Q &= -\frac{3}{2}P_d + \frac{1}{2}P_{v_t} - 2P_{v_s} + \tilde{F}_2 \left[\frac{3}{5}P_d - P_{v_t} + \frac{4\sqrt{2}}{5} \int_0^\infty dr v_t v_s \right] \\
 &+ \int_0^\infty p^2 dp \left\{ \frac{2\sqrt{2}}{5} p^2 \left(u + \frac{1}{\sqrt{8}} w \right) w'' - \frac{p^2}{5} (v_t v_t'' - 2v_s v_s'') \right. \\
 &+ \frac{11\sqrt{2}}{5} p u w' + \frac{9\sqrt{2}}{5} u w + \frac{p^2}{(E+M)^2} \left[-\frac{3\sqrt{2}}{5} p u w' - \frac{1}{3} u^2 - \frac{5\sqrt{2}}{3} u w + \frac{1}{3} w^2 \right] \\
 &+ \frac{\sqrt{6} p}{5(E+M)} \left[(u + \sqrt{2} w) (p v_t' + \frac{2}{3} v_t) + (\sqrt{2} u - w) (p v_s' + \frac{7}{3} v_s) \right] \\
 &+ \frac{3\sqrt{2}}{5} \frac{p^4}{E(E+M)^3} u w \left\} + F_2 \int_0^\infty p^2 dp \left\{ \frac{6\sqrt{2}}{5} (-p u w' + p v_s v_t' - 3 u w) \right. \\
 &+ \frac{p^2}{E(E+M)} \left[-\frac{2}{3} u^2 + \frac{22\sqrt{2}}{15} u w + \frac{1}{15} w^2 + v_t^2 \right] \\
 &+ \frac{4\sqrt{3}}{15} \frac{p}{E+M} \left[(\sqrt{2} u - w) (p v_t' - v_t) + 2(u + \sqrt{2} w) (p v_s' + \frac{3}{2} v_s) \right] \\
 &+ \left. \frac{2}{\sqrt{3}} \frac{p^3}{E(E+M)^2} (\sqrt{2} u - w) v_t \right\} \tag{2.77}
 \end{aligned}$$

We now turn to a discussion of the numerical evaluation of the integrals.

G. Numerical evaluation of the integrals

The two-dimensional integrals in Eq. (2.49) were carried out in a straightforward manner. For a given value of z , a vector of values of the integrand were prepared for each I_i^j on a regularly spaced grid with spacing Δp and maximum value p_{\max} . The integrals were performed using a Simpson's rule over the Δp , Δz grid. At each Q^2 point we first evaluate the integrals using $G_{ES} = 1.0$ (0.0) and $G_{MS} = 0.0$ (1.0), and then from the linear Eq. (2.69) we determine the deuteron body structure functions D_C , D_Q , D_M^E , D_M^M , D_C^{SO} , and D_Q^{SO} . The full deuteron structure functions can then be found quickly for arbitrary nucleon form factors without costly evaluation of the integrals for each case.

Tests were made to establish that the numerical procedure was convergent as a function of the grid sizes Δp and Δz and for the end point p_{\max} . The criterion for convergence was that a given decrease in step size or increase in p_{\max} should change the results for the charge, quadrupole, and magnetic contributions to A , Eq. (1.4), by less than 1% over the entire range of Q^2 from 0 to 200 fm^{-2} . Each parameter was tested independently while the other two were set to a convergent value. The final parameters used were:

$$p_{\max} = 12 \text{ fm}^{-1}$$

$$\Delta p = .04 \text{ fm}^{-1}$$

$$\Delta z = .01$$

The maximum value of $p_{1,2}$ for which momentum space wave functions are required is given by Eq. (2.59) with $z = 1.0$, $p = p_{\max}$, and $Q^2 = Q_{\max}^2$. For $Q_{\max}^2 = 200 \text{ fm}^{-2}$, this gives $p_{1,2} = 24.5 \text{ fm}^{-1}$. A table of regularly

spaced p-space wave functions with grid size $\Delta p = .04 \text{ fm}^{-1}$ was prepared in advance of the structure function calculations. Wave functions at arbitrary p were then obtained by linear interpolation from the table. Approximately 45 seconds of computer time on an IBM 370/168 were required to evaluate all the structure functions at one value of Q^2 for one choice of nucleon form factors.

The numerical values for the deuteron wave functions in position and momentum space for the relativistic models were readily available using the coefficients for the expansion in hankel functions (of imaginary argument) given by Buck and Gross.⁸ The numerical values for the Reid soft core wave functions in momentum space were obtained here by numerical Fourier transformation from the values given in r-space.⁵ For the HM and LF models, values were obtained from an expansion in hankel function (identical to that used in Ref. 8) fit to the original points in momentum space or position space as supplied by the authors. The position space wave functions used in the non-relativistic formulae were obtained by analytic Fourier transform of the momentum space functions.

ACKNOWLEDGEMENTS

Computer work, preparation and publication of this paper were supported in part by the Department of Energy under Contract DE-AC03-76SF00515. R.G.A. wishes to acknowledge support by the National Science Foundation under Grant Numbers GP-16565, MPS75-07325 and PHY-75-15986. C.C. and F.G. wish to acknowledge support by the National Science Foundation under Grant Number PHY-77-07409. During the course of this work, C.C. was an Alfred P. Sloan Foundation Fellow, and gratefully acknowledges this support. It is a pleasure to acknowledge useful conversations with Stanley Brodsky, Ben Chertok, Holger Bech Nielson and Ed Remler.

REFERENCES

1. R. G. Arnold et al., Phys. Rev. Lett. 35, 776 (1975).
2. R. G. Arnold, C. E. Carlson and F. Gross, Phys. Rev. Lett. 38, 1516 (1977).
3. R. Blankenbecler and L. F. Cook, Phys. Rev. 119, 1745 (1960).
4. F. Gross, Phys. Rev. 186, 1448 (1969); Phys. Rev. D10, 223 (1974).
5. R. Reid, Ann. Phys. (N.Y.) 50, 411 (1968).
6. K. Holinde and R. Machleidt, Nucl. Phys. A247, 495 (1975); A256, 479 (1976); A256, 497 (1976). The wave functions from each of these papers will be referred to as HM1, HM2 and HM3, respectively.
7. E. Lomon and H. Feshbach, Ann. Phys. (N.Y.) 48, 94 (1968).
8. W. W. Buck and F. Gross, William and Mary Preprint 78-9 (to be published in Phys. Rev. D).
9. J. S. Levinger, Acta Phys. 33, 135 (1973); T. Brady, E. Tomusiak and J. S. Levinger, Can. J. Phys. 52, 1322 (1974); M. J. Moravcsik and P. Ghosh, Phys. Rev. Lett. 32, 321 (1974).
10. See for example, J. L. Friar, Ann. Phys. (N.Y.) 104, 380 (1977).
11. F. Gross, in Proceedings of the VIII International Conference on Few Body Systems and Nuclear Forces, ed. by H. Zingl et al., p. 46 (Spring-Verlag Lecture Notes in Physics 82, 1978).
12. J. L. Friar, Ann. Phys. (N.Y.) 81, 332 (1973); Phys. Rev. C12, 695 (1975).
13. M. Gari and H. Hyuga, Zeitschrift fur Physik A277, 291 (1976); H. Hyuga and M. Gari, Nucl. Phys. A274, 333 (1976); M. Gari and H. Hyuga, Nucl. Phys. A278, 372 (1977).

14. M. Gari and H. Hyuga, Phys. Rev. Lett. 36, 345 (1976); Nucl. Phys. A264, 409 (1976).
15. R. Adler and S. Drell, Phys. Rev. Lett. 13, 349 (1964); R. Adler, Phys. Rev. 141, 1499 (1966); R. Blankenbecler and J. Gunion, Phys. Rev. D4, 718 (1971); M. Chemtob, E. Moniz, M. Rho, Phys. Rev. C10, 344 (1974); A. Jackson, A. Lande and D. Riska, Phys. Lett. 55B, 23 (1975).
16. W. Fabian and H. Arenhovel, Phys. Rev. Lett. 37, 550 (1976); M. Gari, H. Hyuga and B. Sommer, Phys. Rev. C14, 2196 (1976).
17. D. Coward et al., Phys. Rev. Lett. 20, 292 (1968).
18. W. Bartel et al., Phys. Lett. 33B, 245 (1970).
19. W. Bartel et al., Nucl. Phys. B58, 429 (1973); K. Hansen et al., Phys. Rev. D8, 753 (1973).
20. S. Galster et al., Nucl. Phys. B32, 221 (1971).
21. V. E. Krohn and G. R. Ringo, Phys. Rev. 148, 1303 (1966).
22. F. Iachello, A. Jackson and A. Lande, Phys. Lett. 43B, 191 (1973).
23. D. Soper, Phys. Rev. D15, 1141 (1977). See also Appendix C of the second of Ref. 24.
24. S. Brodsky and G. Farrar, Phys. Rev. Lett. 31, 1153 (1973); Phys. Rev. D11, 1309 (1975); Y. Matveev, R. Muradrian and A. Tavkhelidze, Nuovo Cimento Lett. 7, 719 (1973).
25. S. Brodsky and B. Chertok, Phys. Rev. Lett. 37, 269 (1976); Phys. Rev. D14, 3003 (1976).
26. Z. Ezawa, Nuovo Cimento 23A, 271 (1974).
27. This is suggested if vector meson dominance is to give a dipole fit to the nucleon form factor.

28. F. Coester and A. Ostabee, Phys. Rev. C11, 1836 (1975); F. Gross, Proceedings of the Quebec Conference, ed. by R. O. Slobodrian et al., p. 782 (1974).
29. F. L. Gross, Phys. Rev. 142, 1025 (1966); B. Casper and F. Gross, Phys. Rev. 155, 1607 (1967).
30. Our conventions follow J. Bjorken and S. Drell, Relativistic Quantum Mechanics (McGraw-Hill, New York, 1964).
31. H. F. Jones, Nuovo Cimento 26, 790 (1962).
32. F. Gross, Phys. Rev. 140, B410 (1965).

FIGURE CAPTURES

Fig. 1. (a) The relativistic Feynman diagram which describes the impulse approximation (RIA). (b) Three nonrelativistic time ordered diagrams included in the RIA. The lines moving backward in time are anti-particles. (c) and (d) Two examples of processes that are not included in the RIA. Diagram (c) is a meson exchange contribution and diagram (d) is an isobar contribution.

Fig. 2. Numerical evaluation of the relativistic formulae of this paper for $A(Q^2)$ using various two-component deuteron wave functions. The models included are: Reid soft core, labeled RSC (Ref. 5); three Holinde-Macheidt models, labeled HM1, HM2, HM3 (Ref. 6); and two Lomon-Feshbach models with different percent D states (Ref. 7). For comparison the solid line labeled RSC-NR, is the result obtained from the nonrelativistic formulae evaluated with Reid soft core wave functions. Dipole nucleon form factors were used in every case. The data for $A(Q^2)$ are from Ref. 1.

Fig. 3. Numerical evaluation of the relativistic formulae for $B(Q^2)$ using the same wave functions as in Fig. 2.

Fig. 4. The charge form factor contribution to $A(Q^2)$ evaluated using the relativistic formulae and the same wave functions as in Fig. 2.

Fig. 5. The quadrupole form factor contribution to $A(Q^2)$ evaluated using the relativistic formulae and the same wave functions as in Fig. 2.

Fig. 6. The recoil deuteron tensor polarization $T(Q^2)$ evaluated using the relativistic formulae and the same wave functions as in Fig. 2.

Fig. 7. Numerical evaluation of the relativistic formulae for $A(Q^2)$ using various relativistic deuteron wave functions given in Ref. 8. The parameter λ which differentiates the models is described in the text. For comparison, the solid line labeled RSC-NR, is the result obtained from nonrelativistic formulae evaluated with Reid soft core wave functions. Dipole nucleon form factors were used everywhere. The data points for $A(Q^2)$ are from Ref. 1.

Fig. 8. Numerical evaluation of the relativistic formulae for $B(Q^2)$ using the same wave functions as in Fig. 7.

Fig. 9. The charge form factor contribution to $A(Q^2)$ evaluated using the same wave functions as in Fig. 7.

Fig. 10. The quadrupole form factor contribution to $A(Q^2)$ evaluated using the same wave functions as in Fig. 7.

Fig. 11. The recoil deuteron tensor polarization $T(Q^2)$ evaluated using the relativistic formulae and the same wave functions as in Fig. 7.

Fig. 12. (a) the S state, (b) the D state, and the two P state deuteron wave functions, (c) v_t and (d) v_s , for all the models used in this paper. Note that the vertical scale of the S state wave functions is different from the scale of the others. The wave functions are all precisely defined in Section II.

Fig. 13. Relativistic corrections to the structure function $A(Q^2)$. The ratio of A calculated with the relativistic formulae of this paper to A calculated with the usual nonrelativistic formulae is given for each model shown in Fig. 2. Dipole nucleon form factors were used.

Fig. 14. Relativistic corrections to the fundamental form factors G_C , G_Q and G_M . In parts (a), (c) and (e) we show the relativistic and nonrelativistic result as well as the difference between the relativistic and nonrelativistic result for the HM3 model only. In parts (b), (d) and (f) the differences for all of the models of Fig. 2 are shown. Dipole nucleon form factors were used.

Fig. 15. Relativistic corrections to the structure function $A(Q^2)$.

(a) The ratio R_{Full} defined in the text is given for each model shown in Fig. 7. (b) The three ratios R_{None} , R_{Lin} and R_{Full} are compared for the $\lambda = 1$ model of Ref. 8. Dipole nucleon form factors were used.

Fig. 16. Relativistic corrections to the fundamental form factors G_C , G_Q and G_M . In parts (a), (c) and (e) we show for the $\lambda = 1$ model, each of the four possible ways of calculating the form factor discussed in the text, labeled NR, None, Lin and Full, together with the difference between the Full result and the NR result. In parts (b), (d) and (f) we show the differences for each of the relativistic models in Fig. 7. The mixing parameter λ which differentiates these models is described in the text and in Ref. 8. Dipole nucleon form factors were used.

Fig. 17. Effect of various nucleon form factors on the deuteron structure functions $A(Q^2)$, evaluated using the relativistic formulae and the two-component Holinde-Machleidt model HM3 (Ref. 6). The various nucleon form factors are: Dipole from Eq. (1.6);

IJL from Ref. 22; Best Fit described in the text; Best Fit + $G_{En} = 0$, same as the Best Fit form factors except the neutron electric form factors G_{En} was set to zero; Dipole + $F_{1n} = 0$, the same as Eq. (1.6), but with the neutron Dirac form factor F_{1n} set equal to zero.

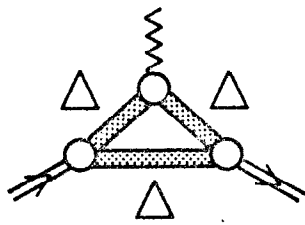
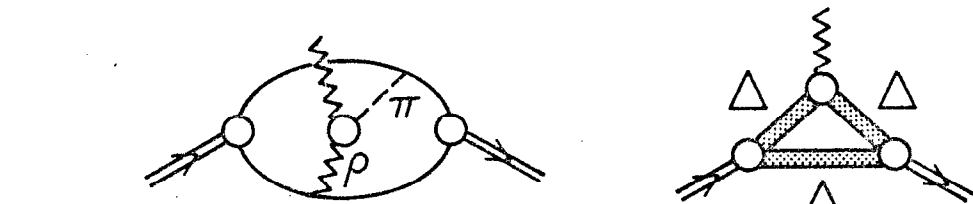
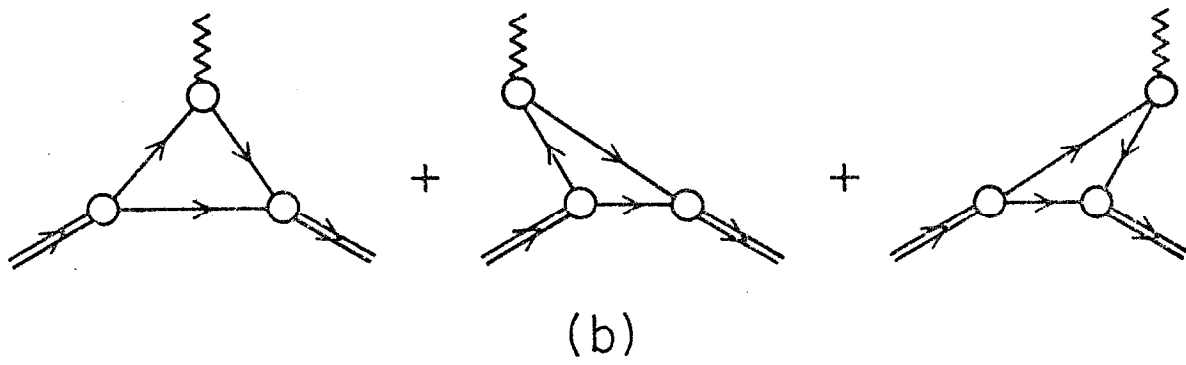
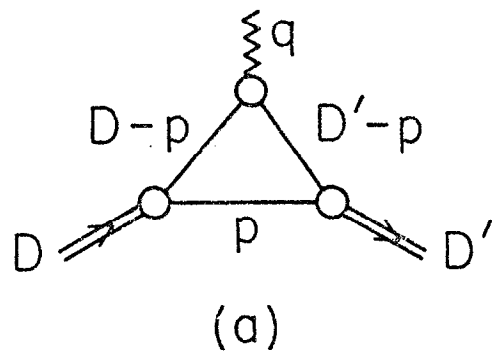
Fig. 18. Effect of various nucleon form factors on the deuteron structure function $B(Q^2)$ evaluated using the HM3 two-component model in the relativistic formulae and the same nucleon form factors as in Fig. 17.

Fig. 19. Effect of various nucleon nucleon form factors on the deuteron structure function $A(Q^2)$ evaluated using the relativistic wave function model for $\lambda = 0.4$ (Ref. 8) and the same nucleon form factors as in Fig. 17.

Fig. 20. Effect of various nucleon form factors on the deuteron structure function $B(Q^2)$ evaluated using the relativistic wave function model for $\lambda = 0.4$ (Ref. 8) and the same nucleon form factors as in Fig. 17.

Fig. 21. Various estimates for the neutron form factor G_{En} used in this paper. The curves are: IJL from Ref. 22; Best Fit described in the text; $F_{1n} = 0$ leading to the form given in Eq. (1.8). For comparison, the dipole curve G_{Ep} is also shown.

Fig. 22. Comparison of our result with various approximations discussed in the text. The ratio of A calculated with various approximate relativistic formulae to A calculated with the usual non-relativistic formulae is displayed. All curves are for the Reid soft core wave functions with dipole nucleon form factors.



5-79

3085A31

Fig. 1

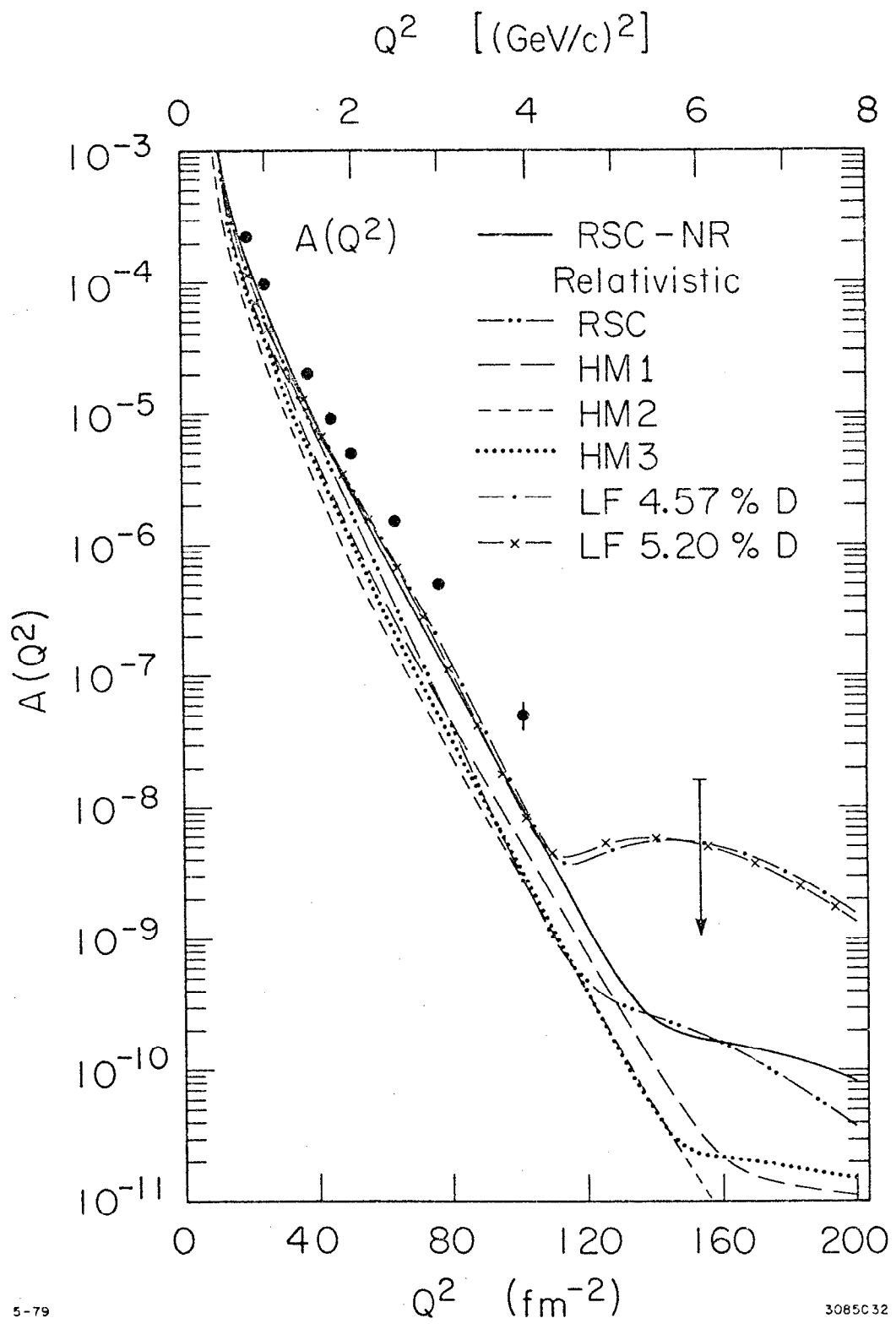


Fig. 2

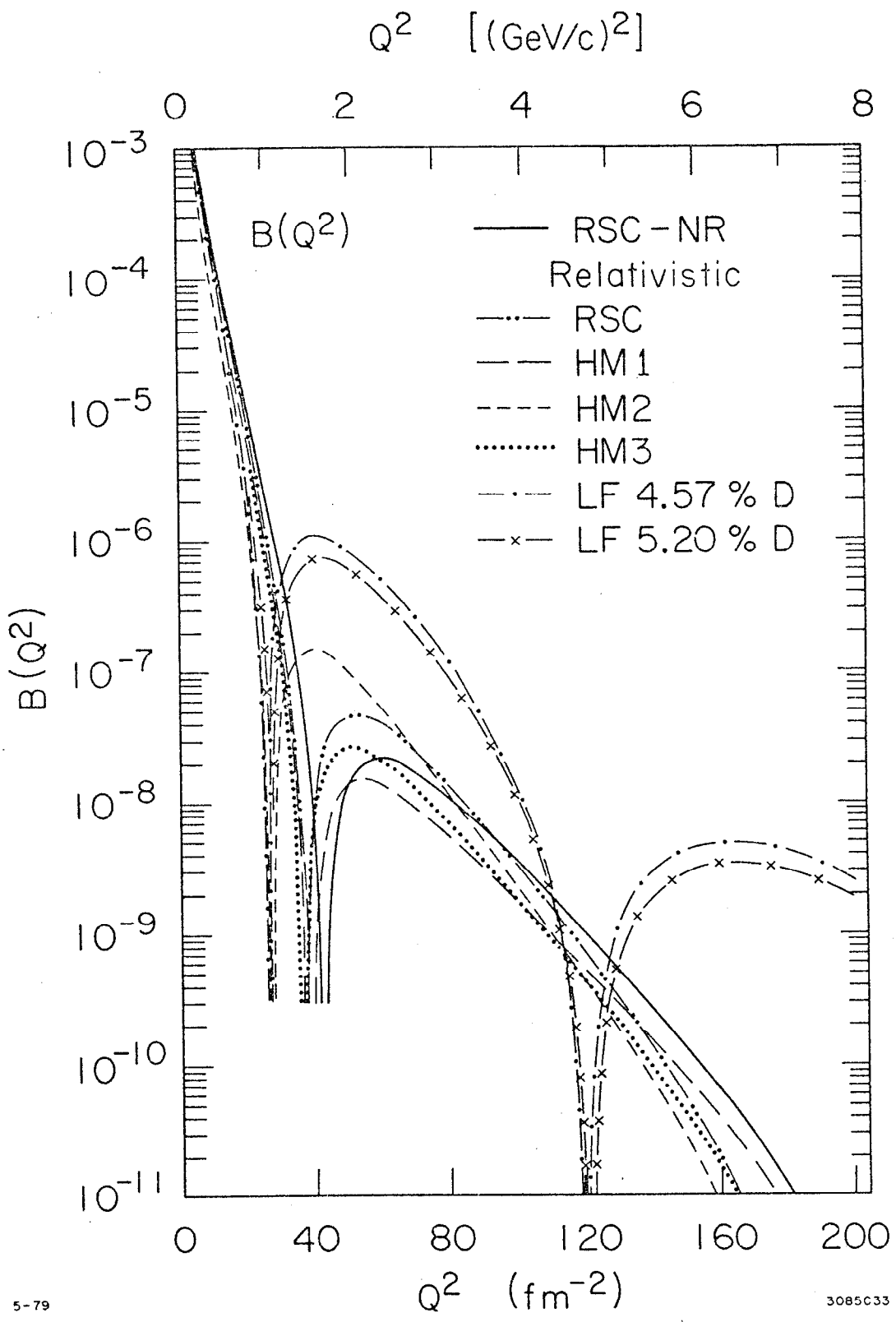
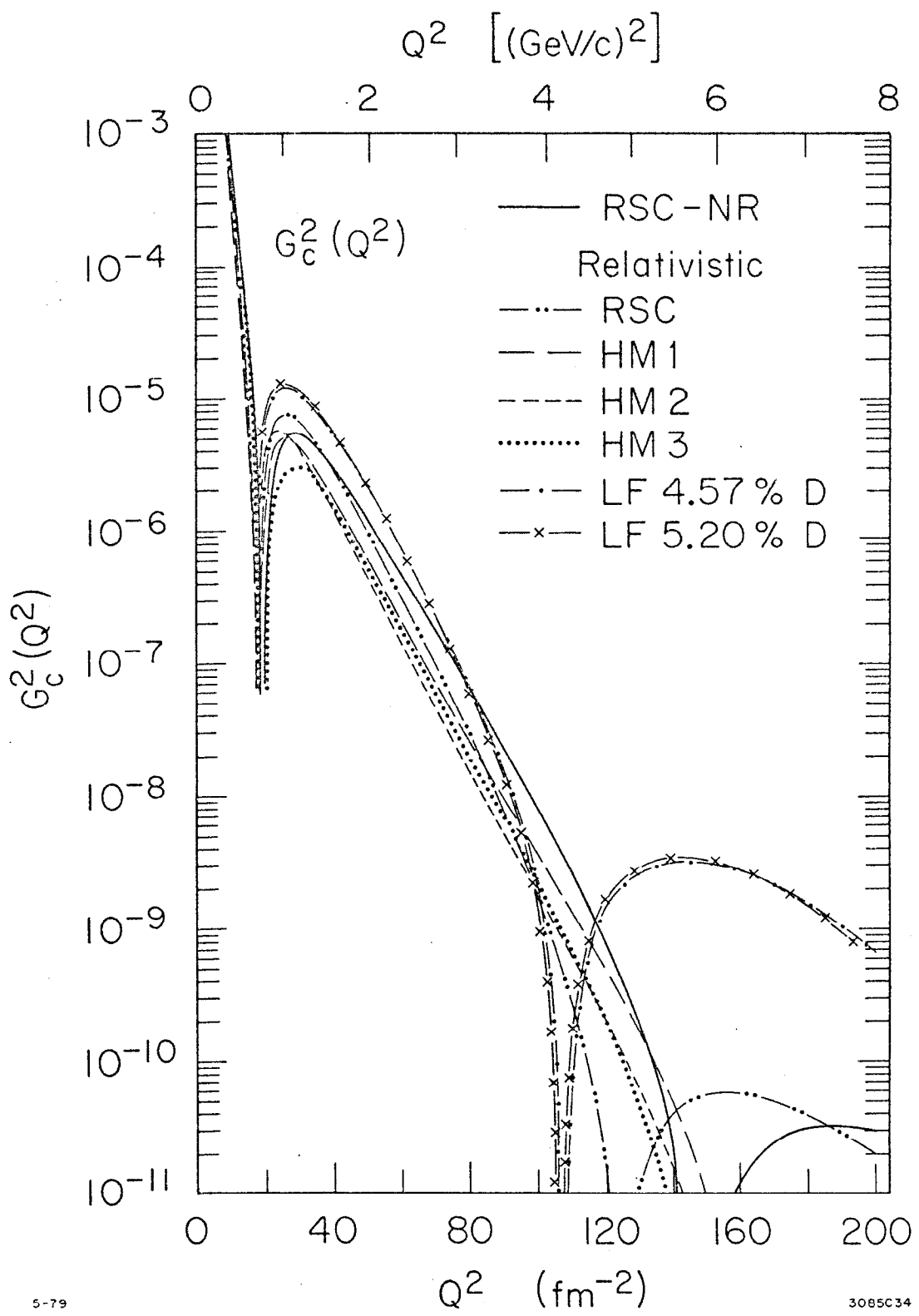


Fig. 3



5-79

3085C34

Fig. 4

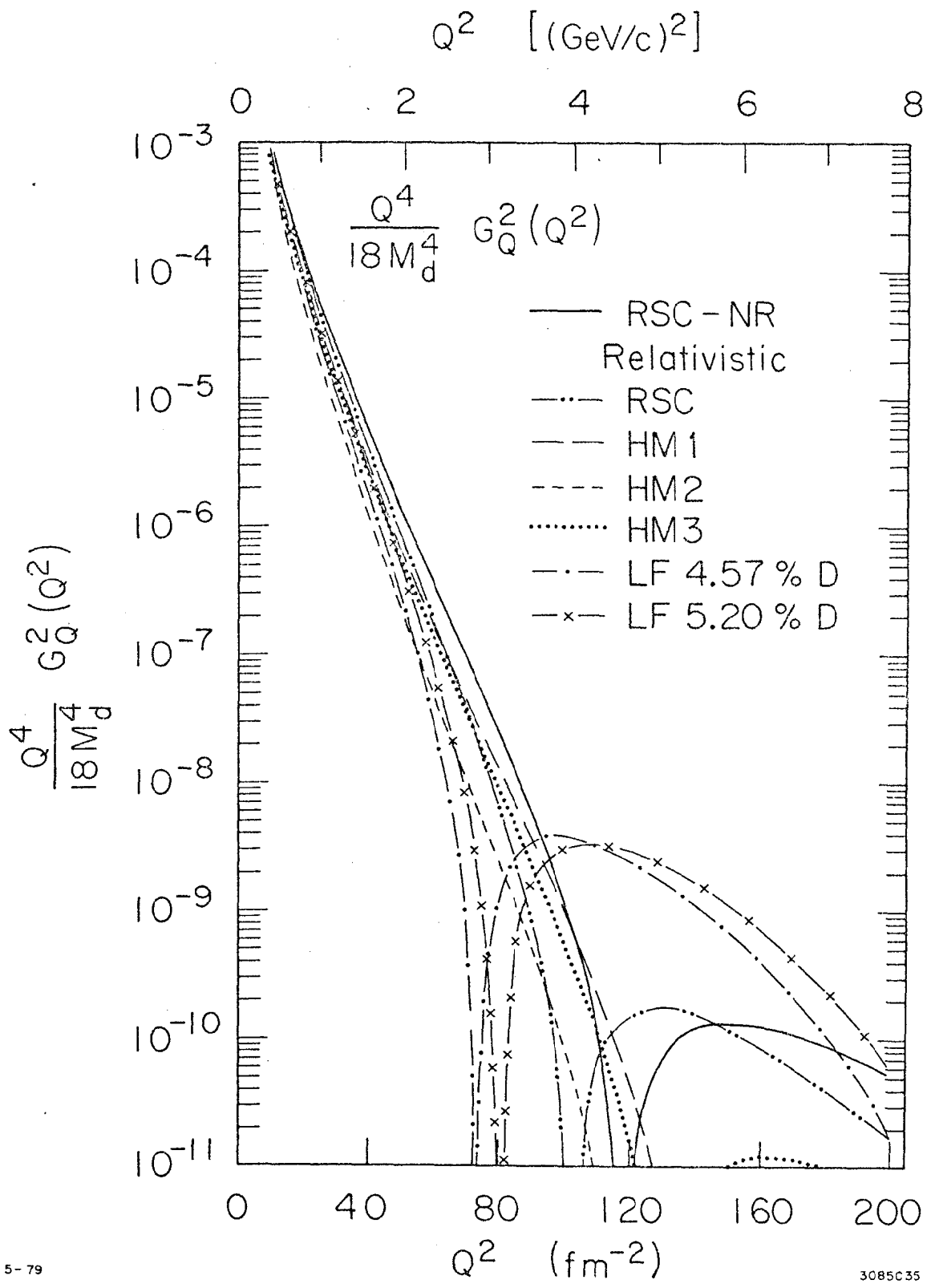


Fig. 5

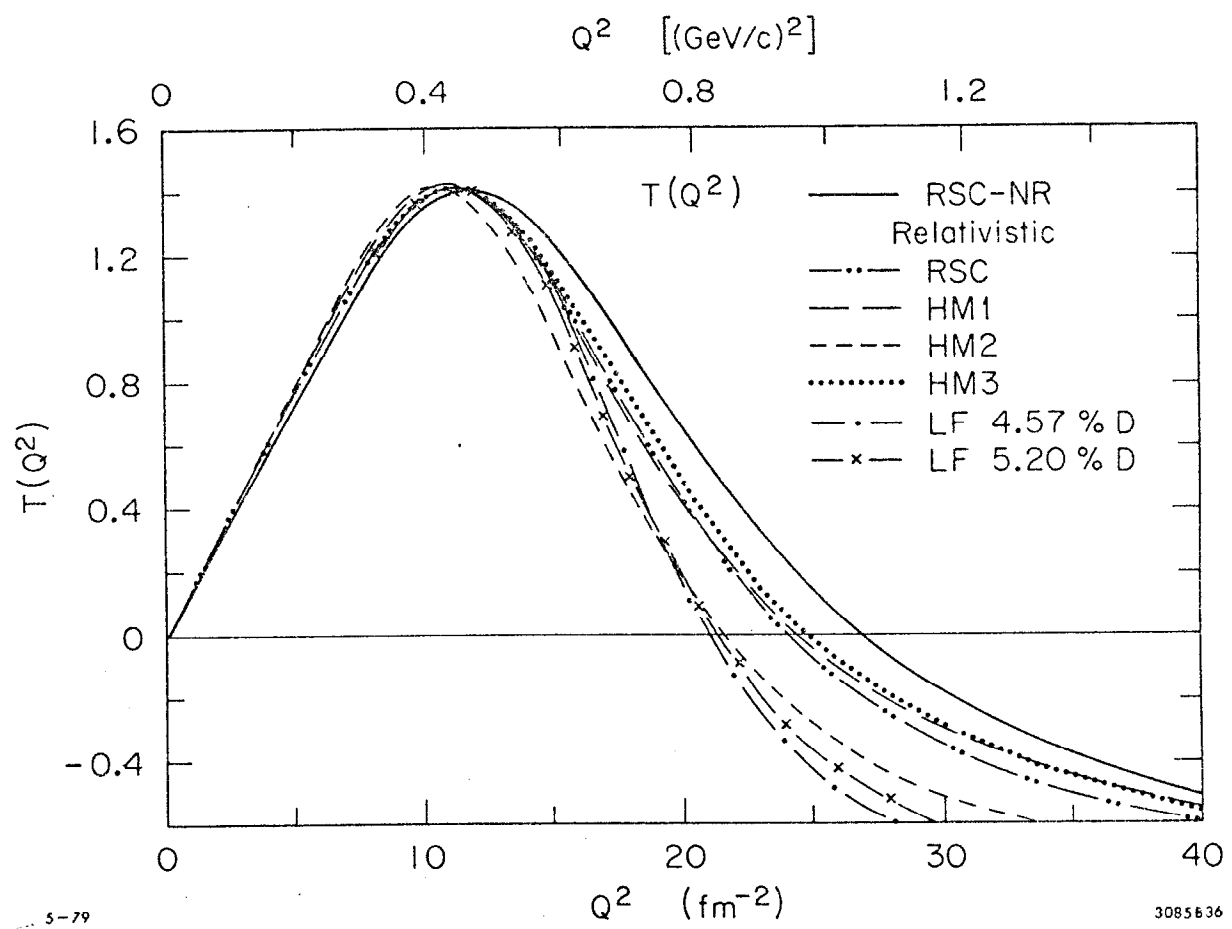


Fig. 6

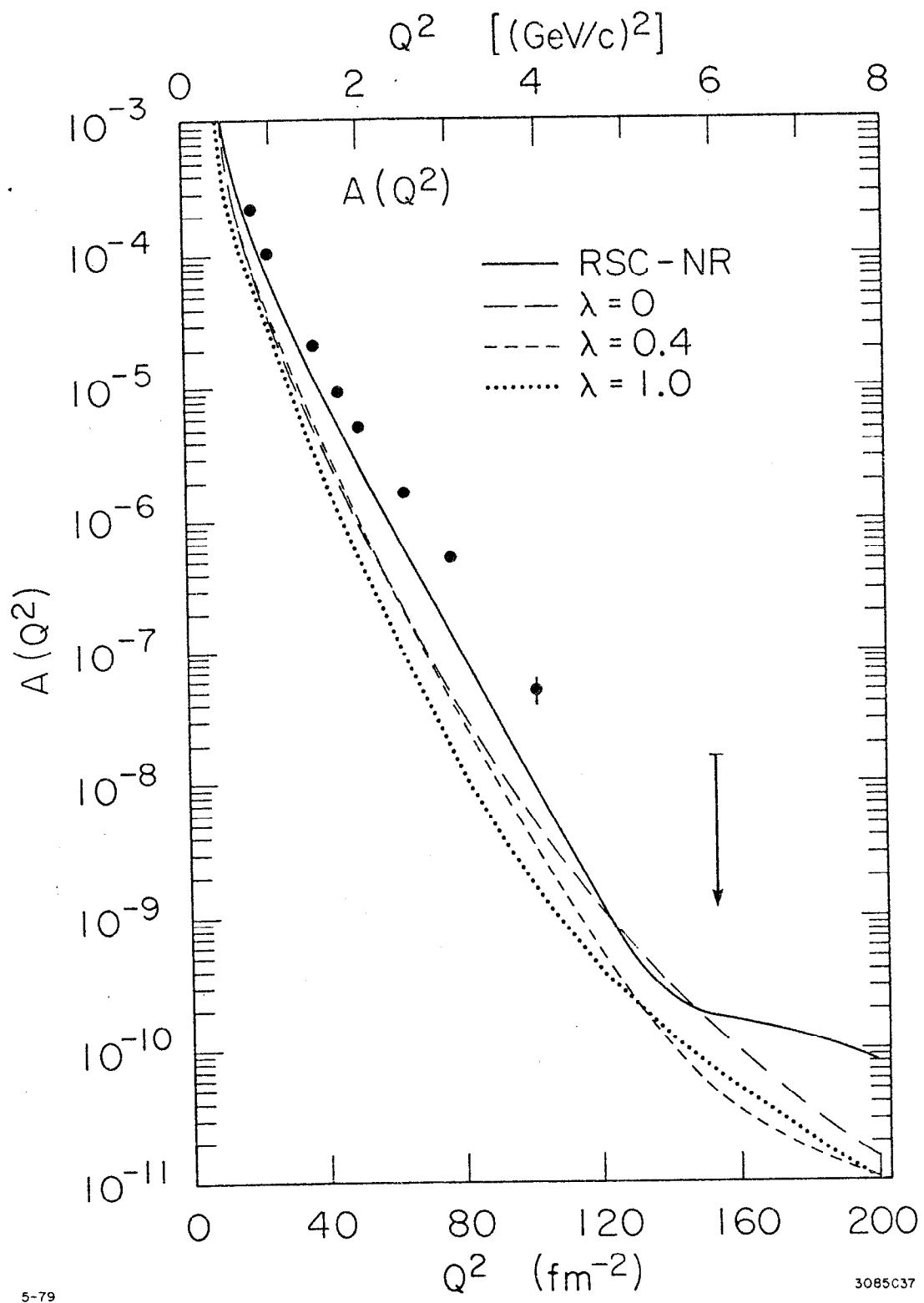


Fig. 7

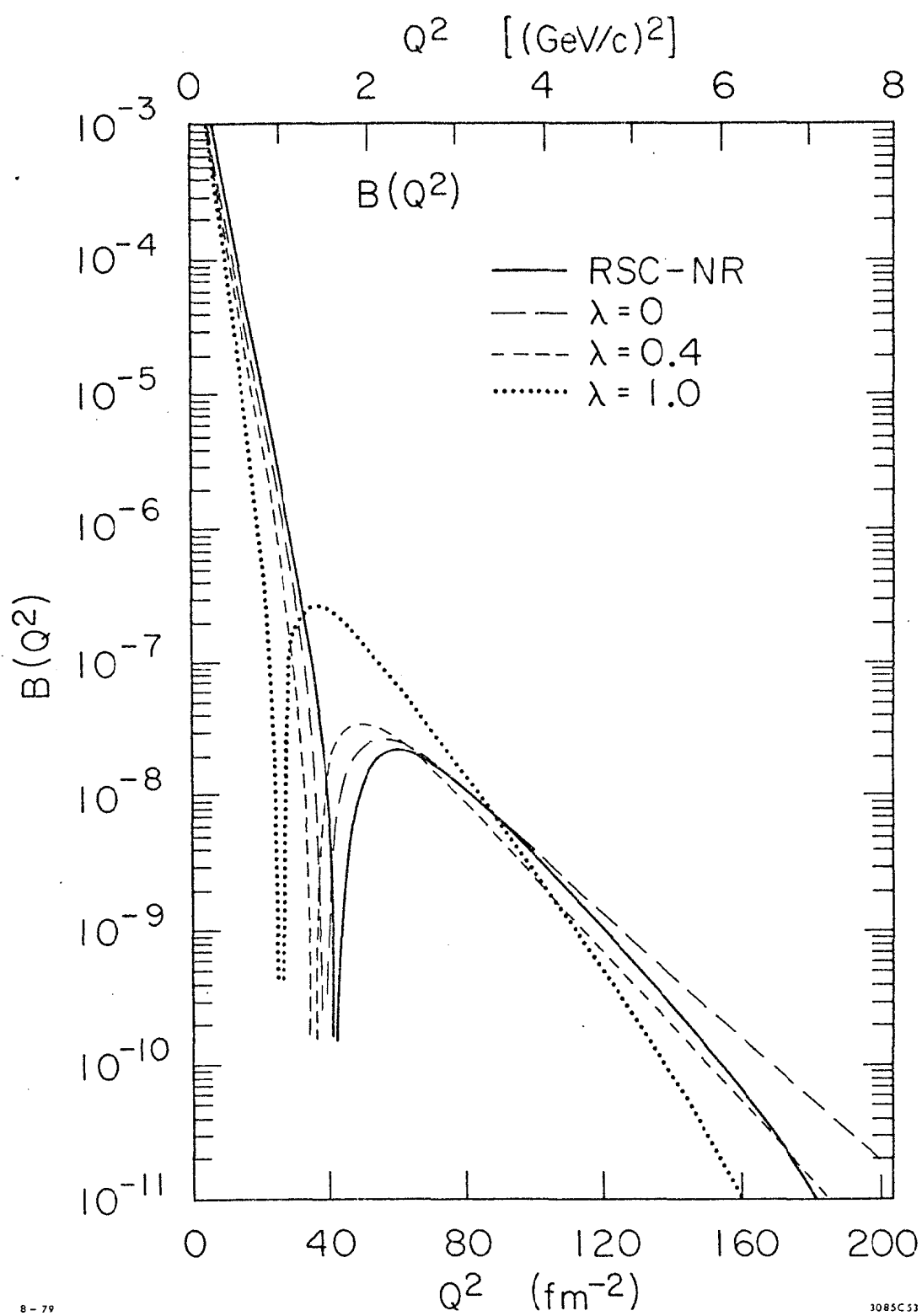


Fig. 8

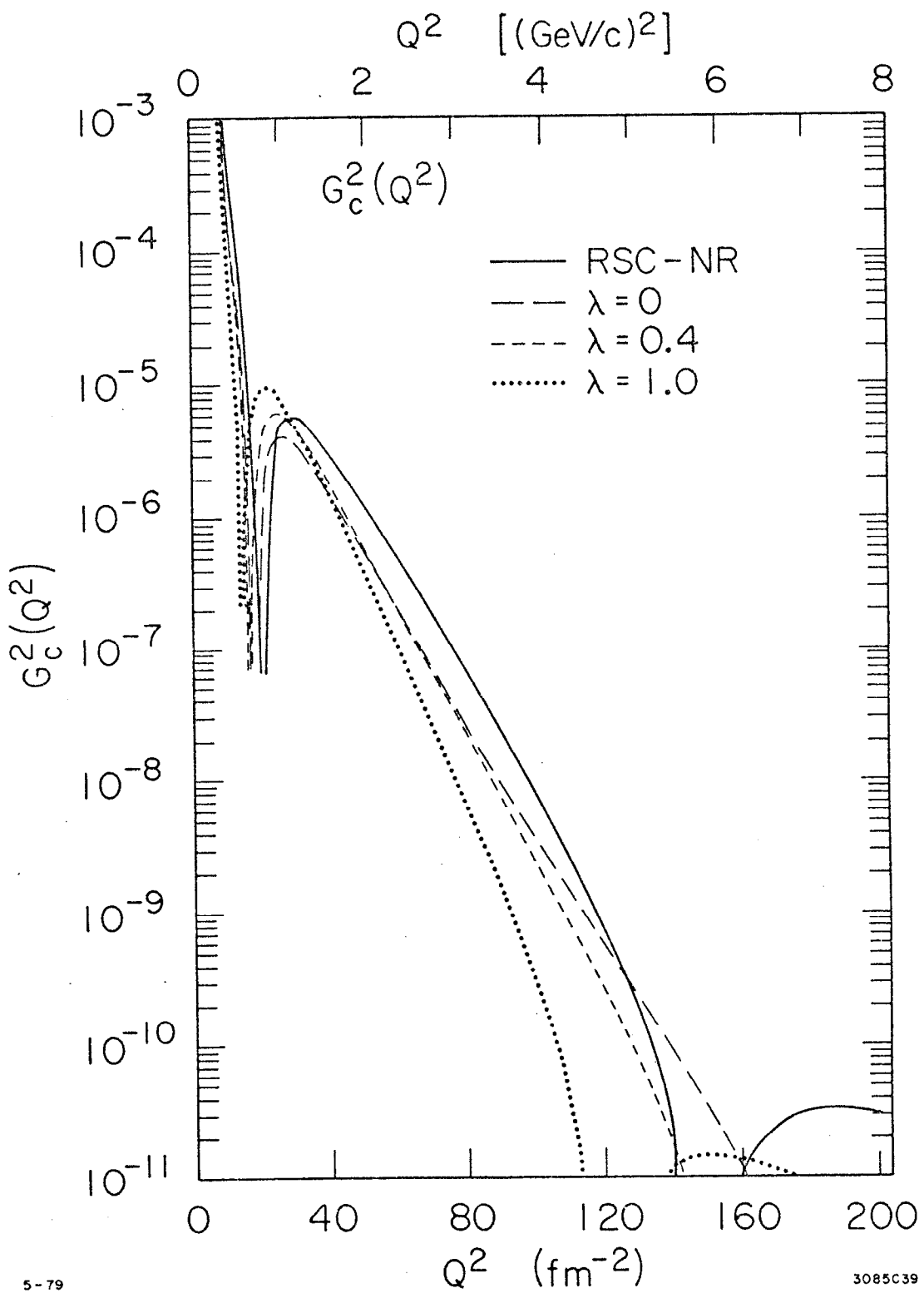


Fig. 9

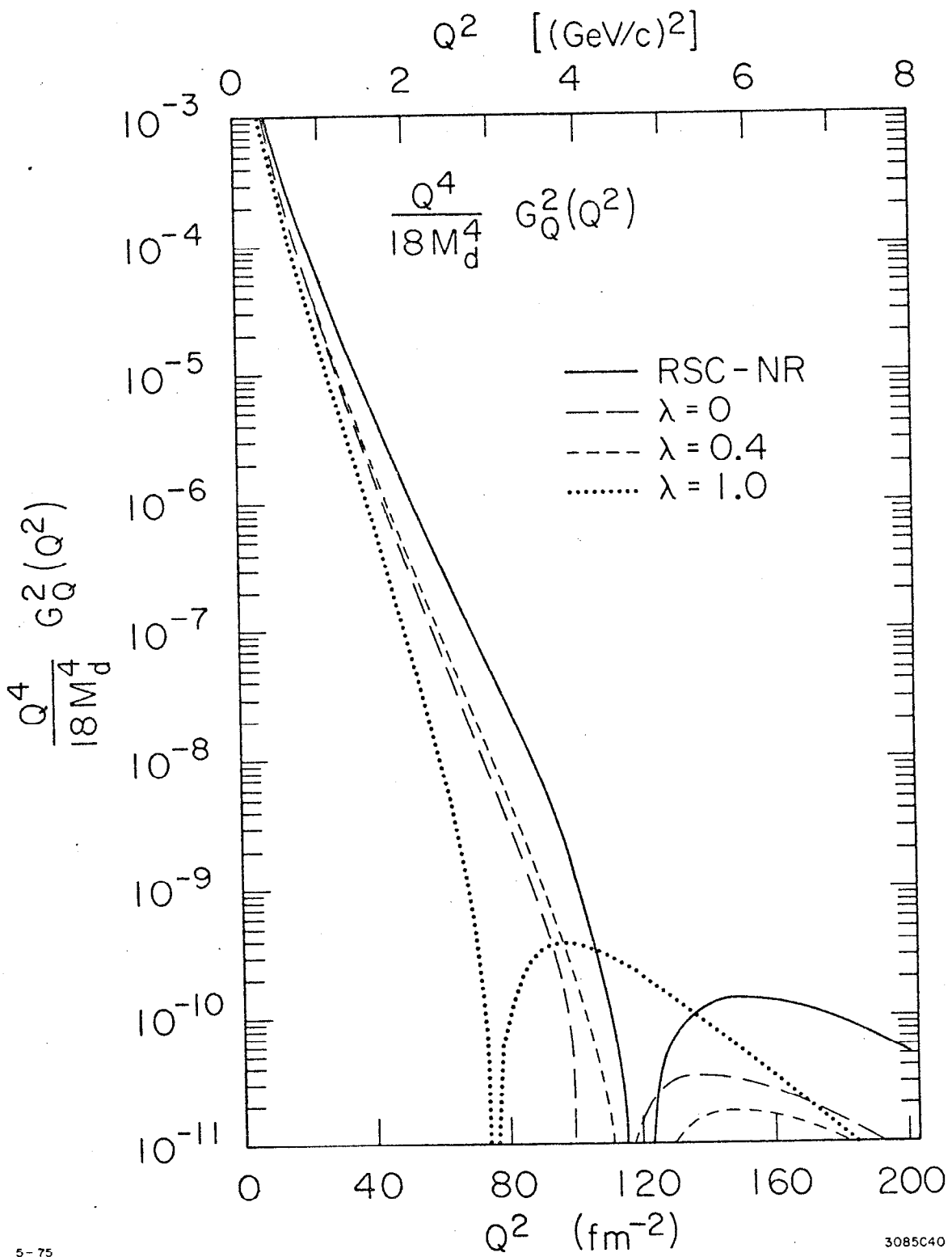


Fig. 10

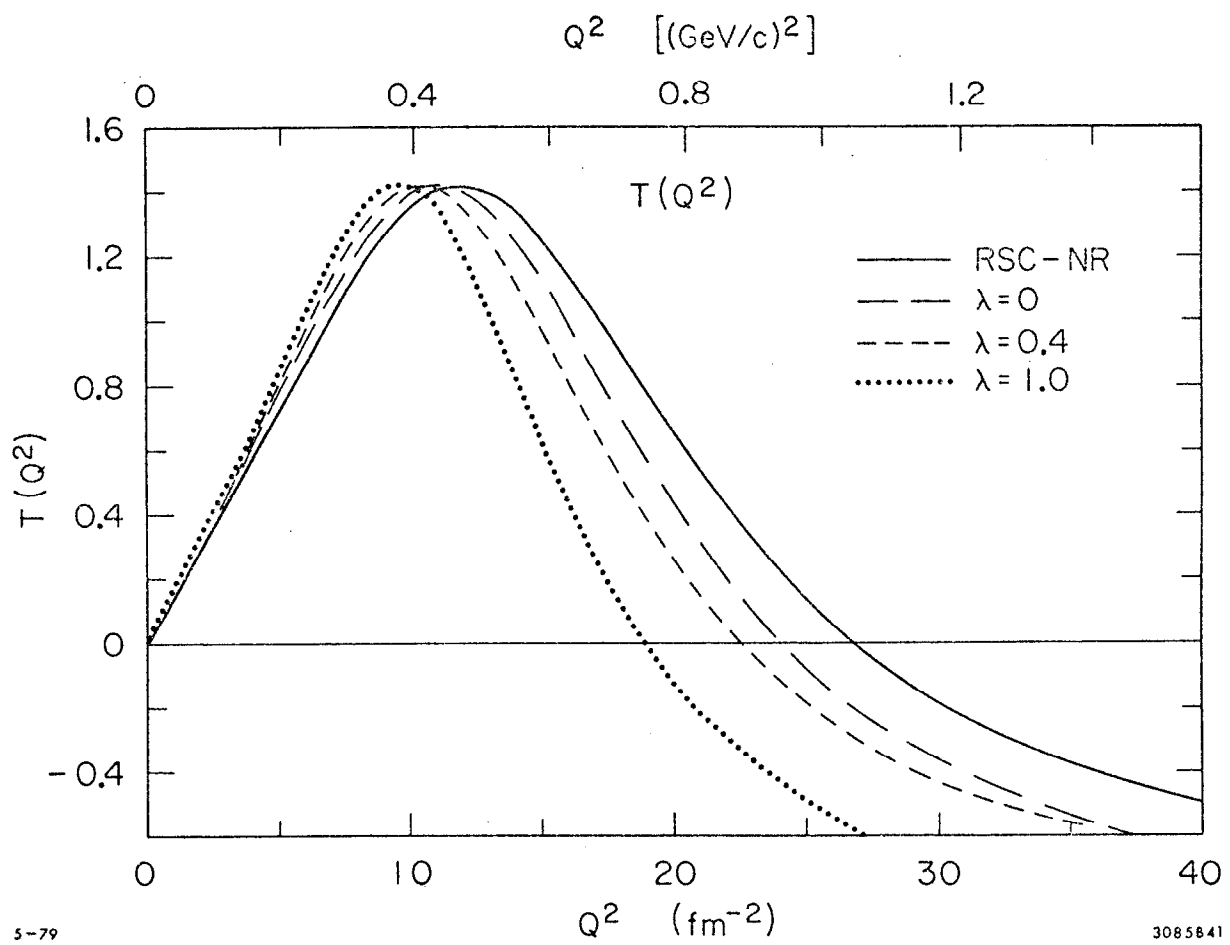


Fig. 11

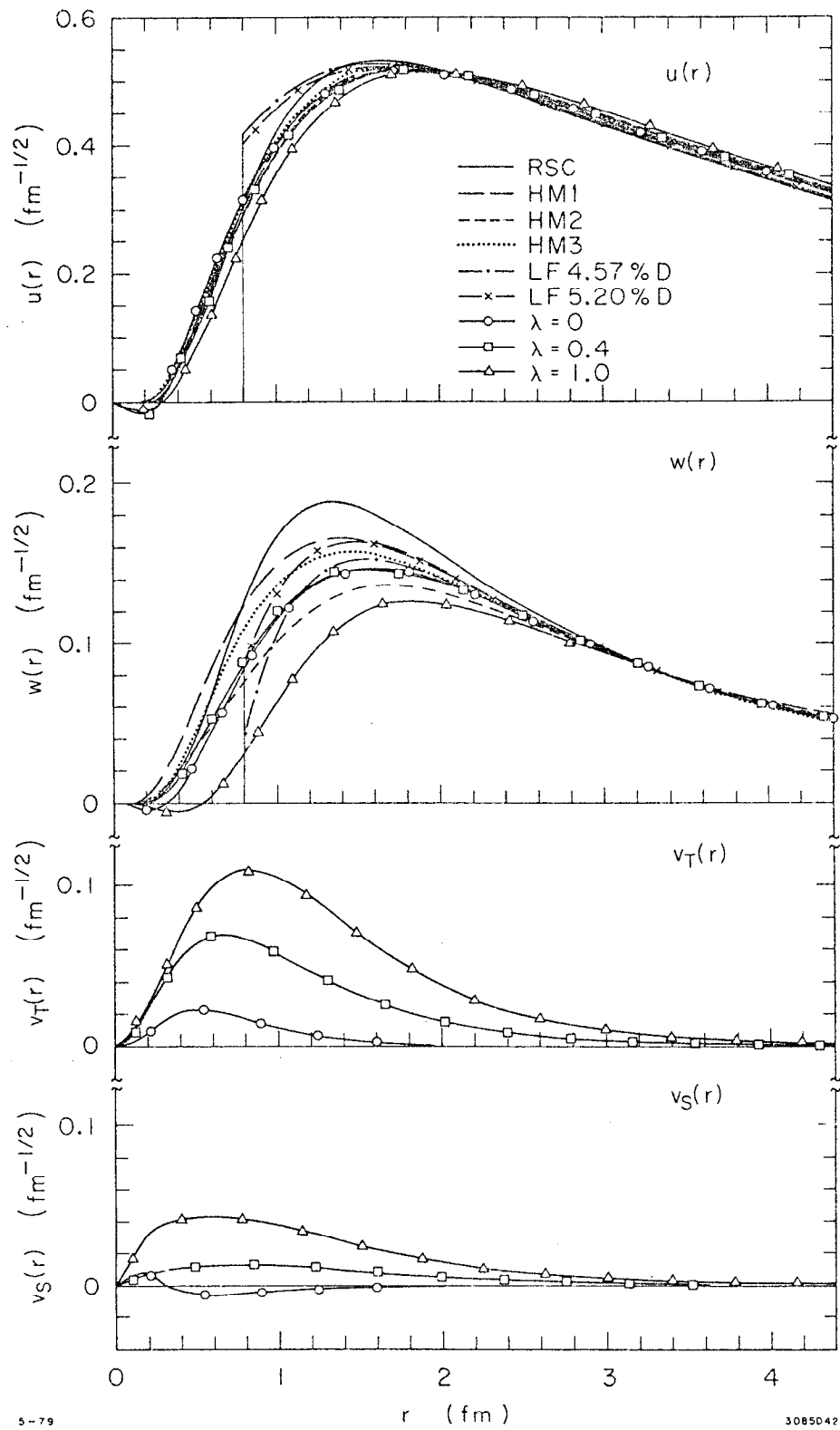


Fig. 12

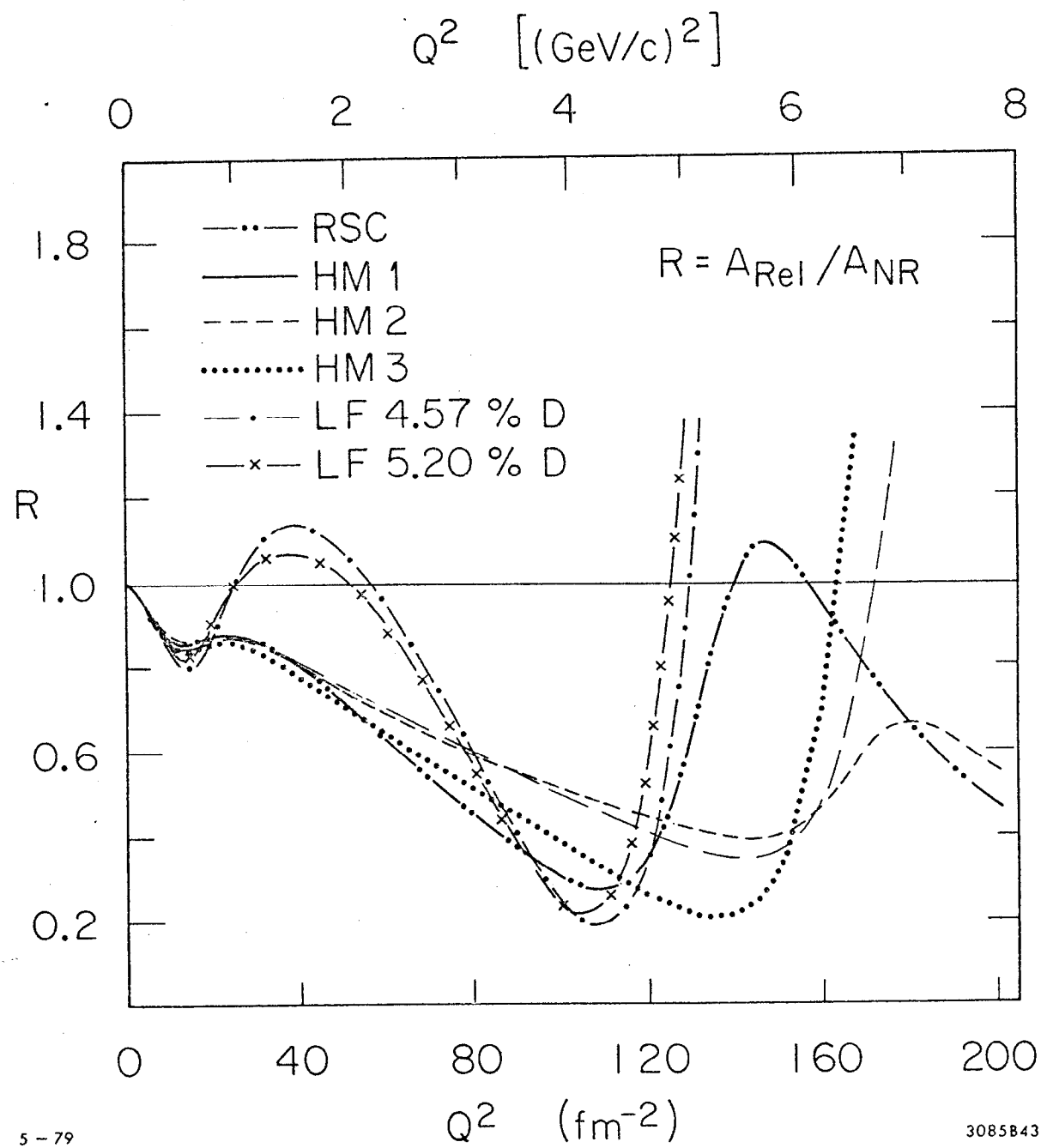


Fig. 13

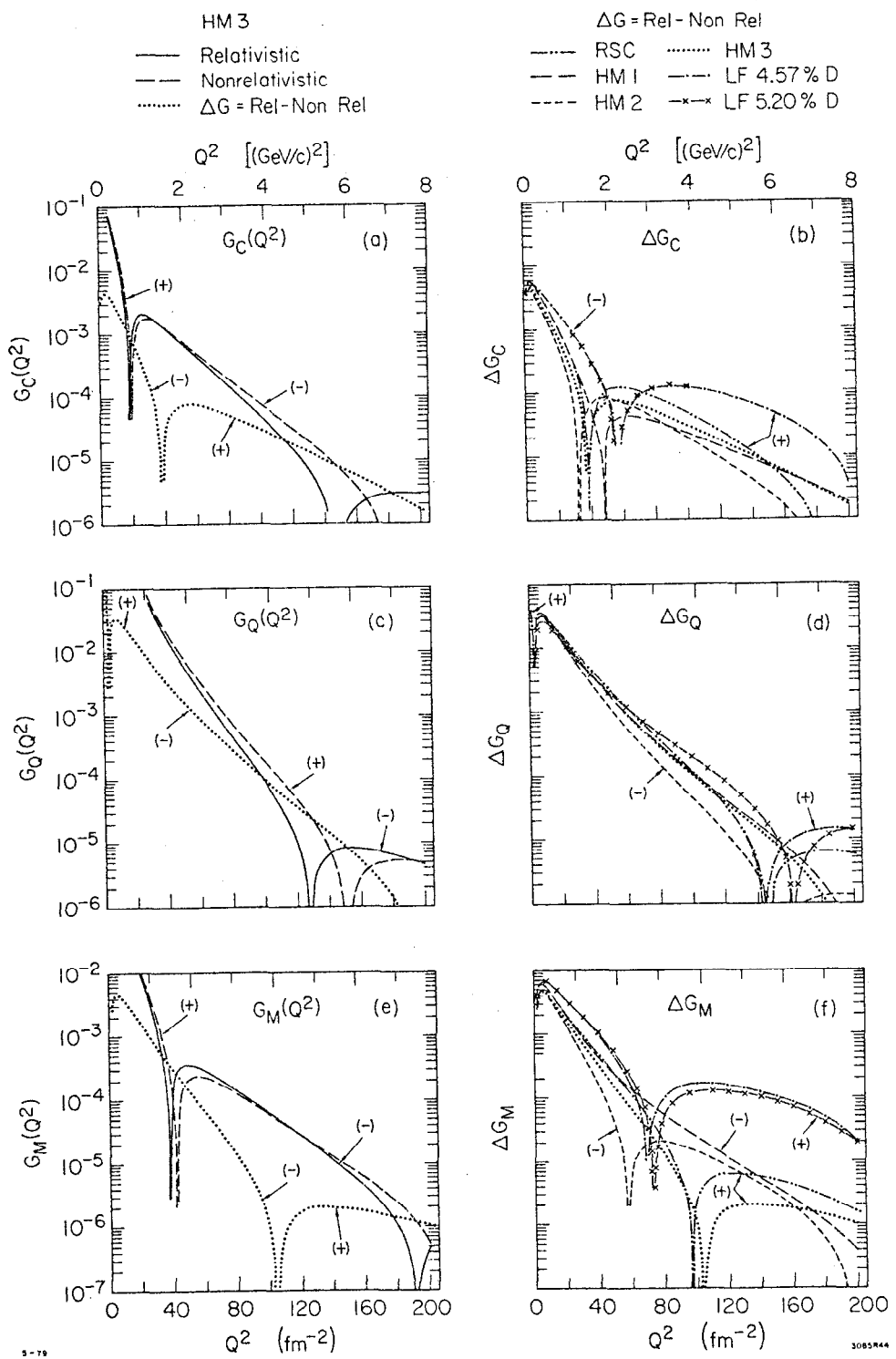


Fig. 14

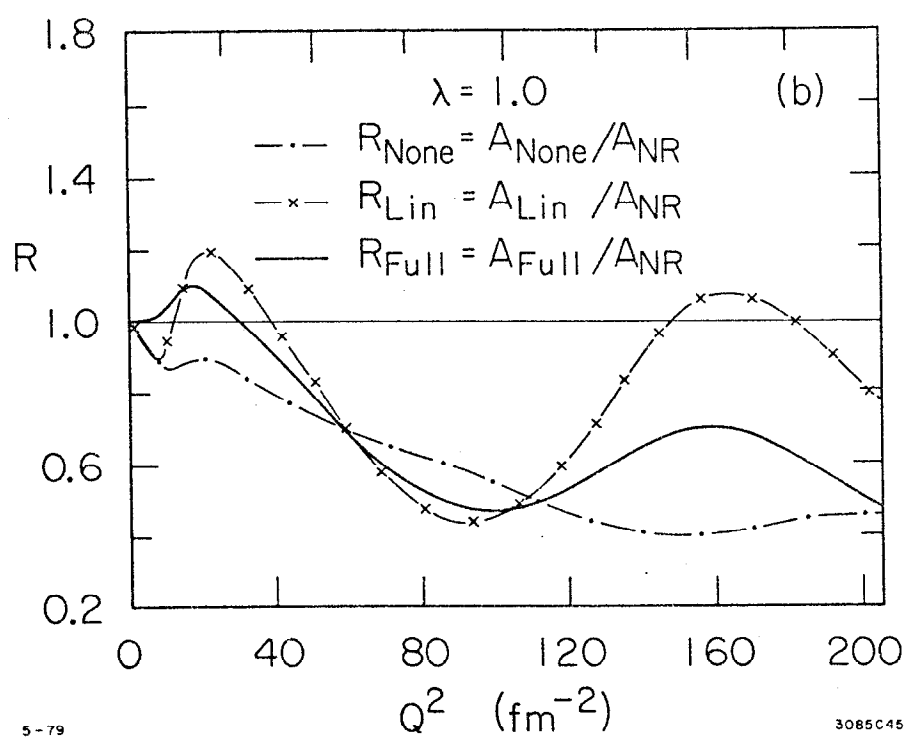
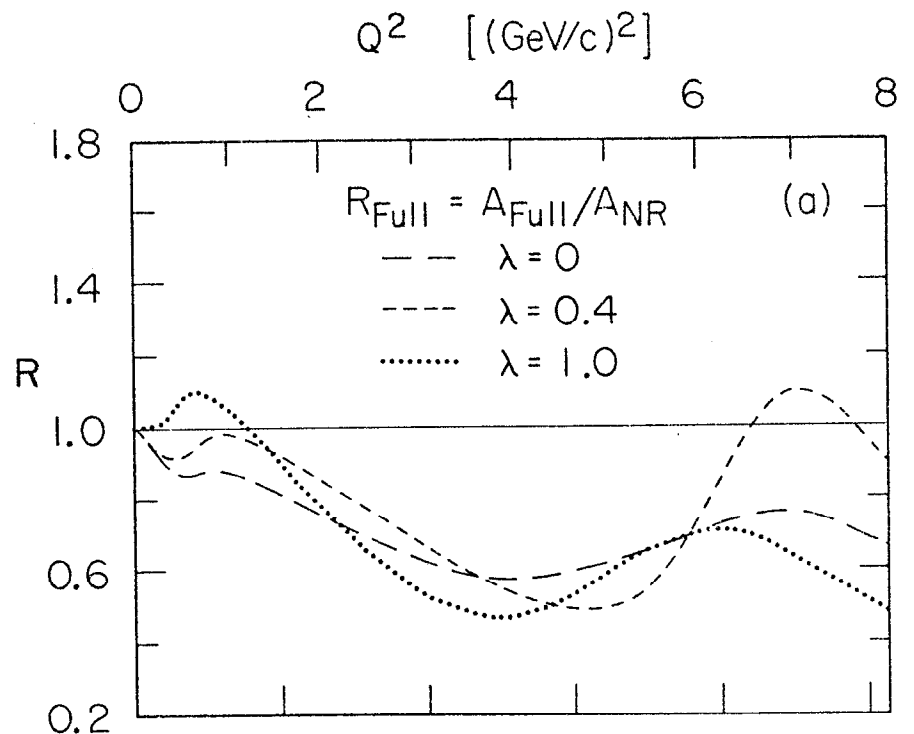


Fig. 15

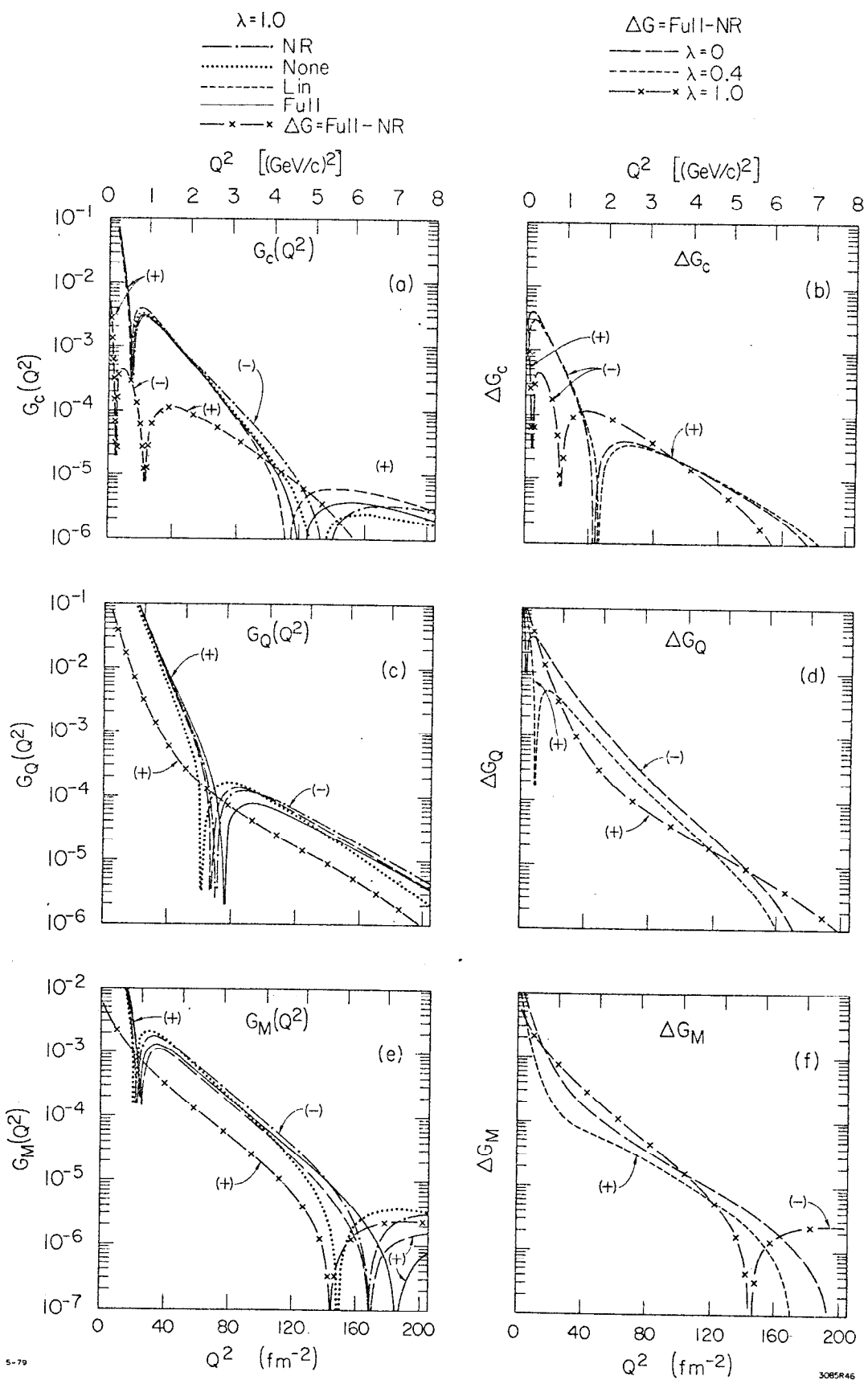


Fig. 16

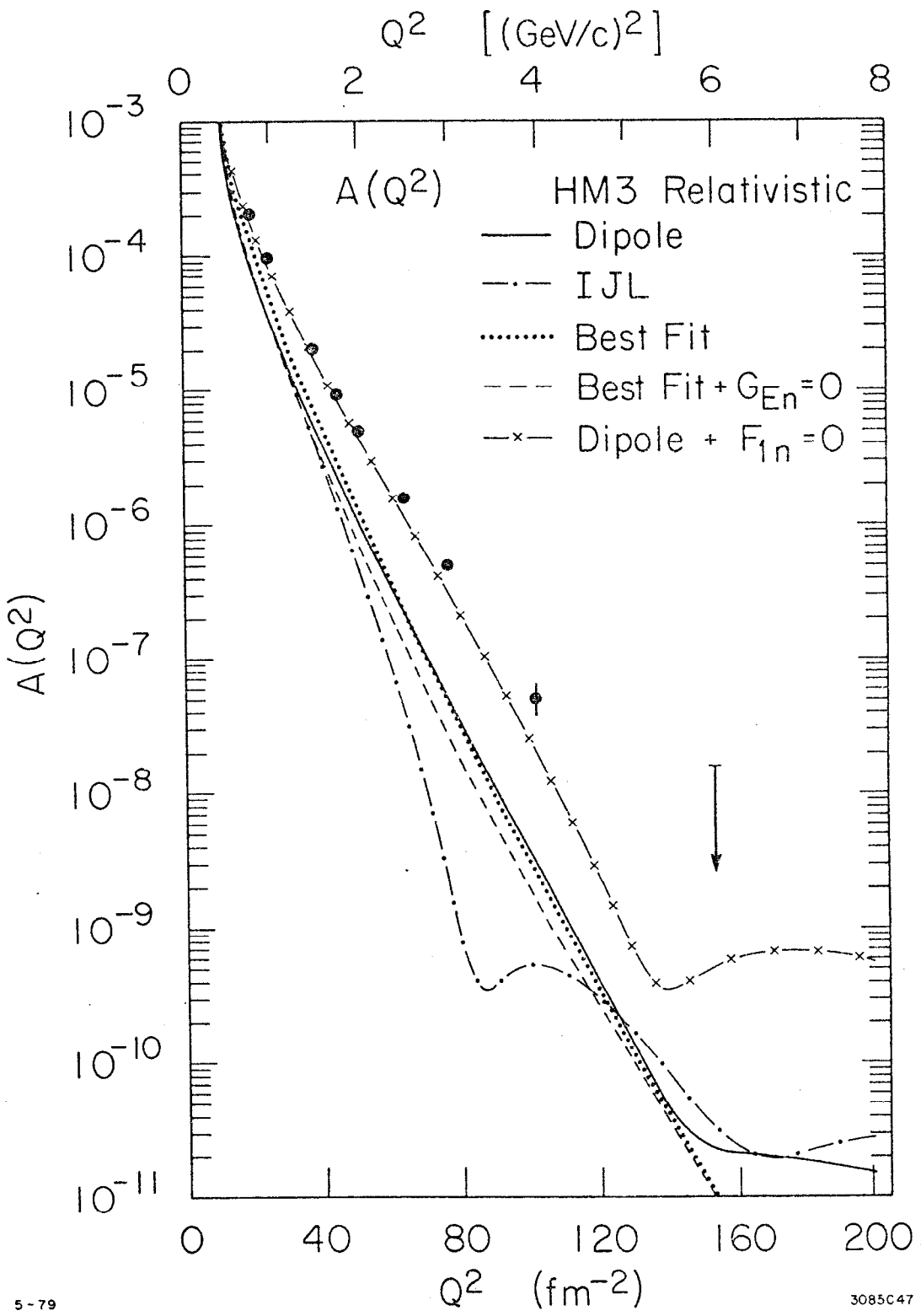


Fig. 17

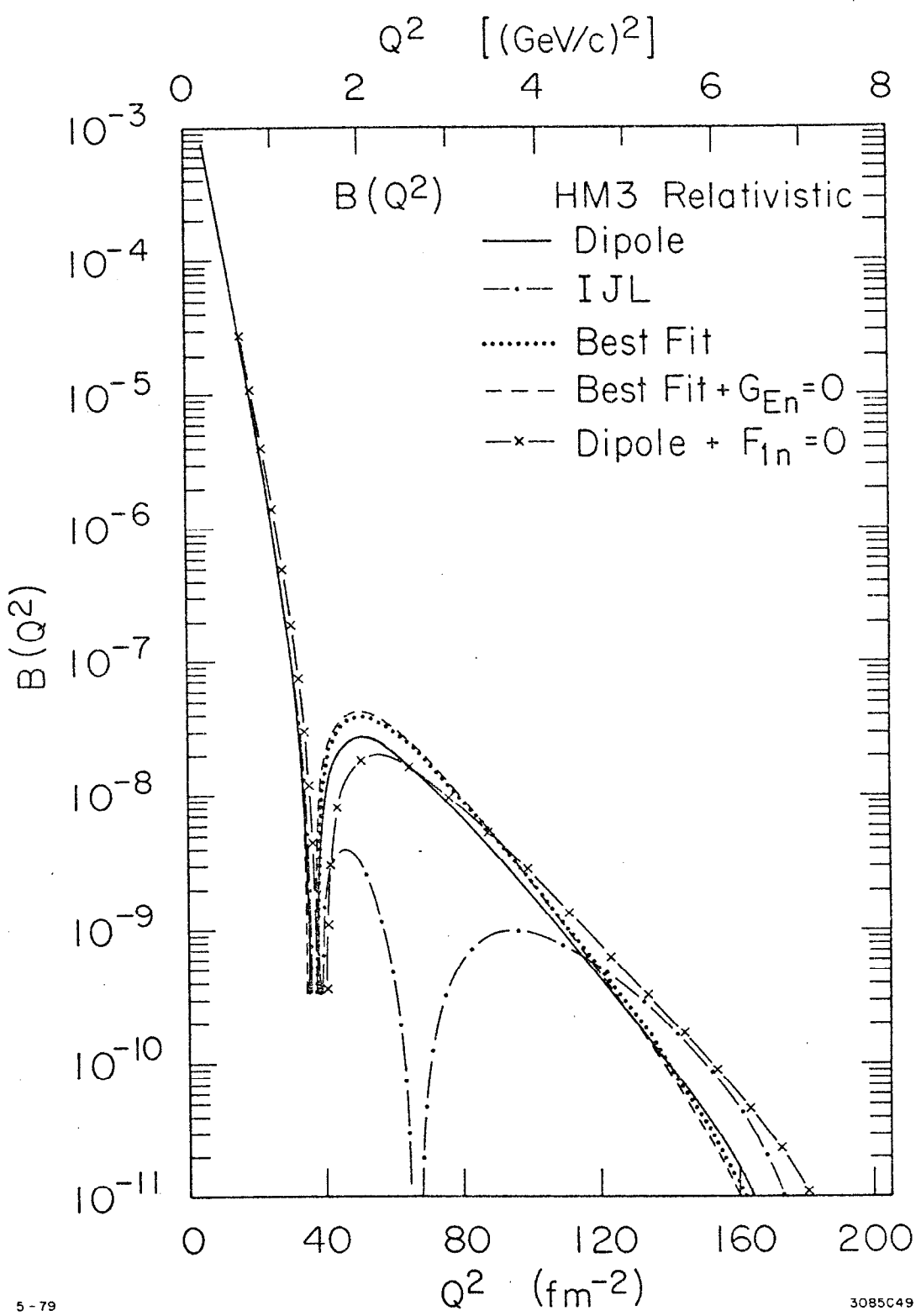


Fig. 18

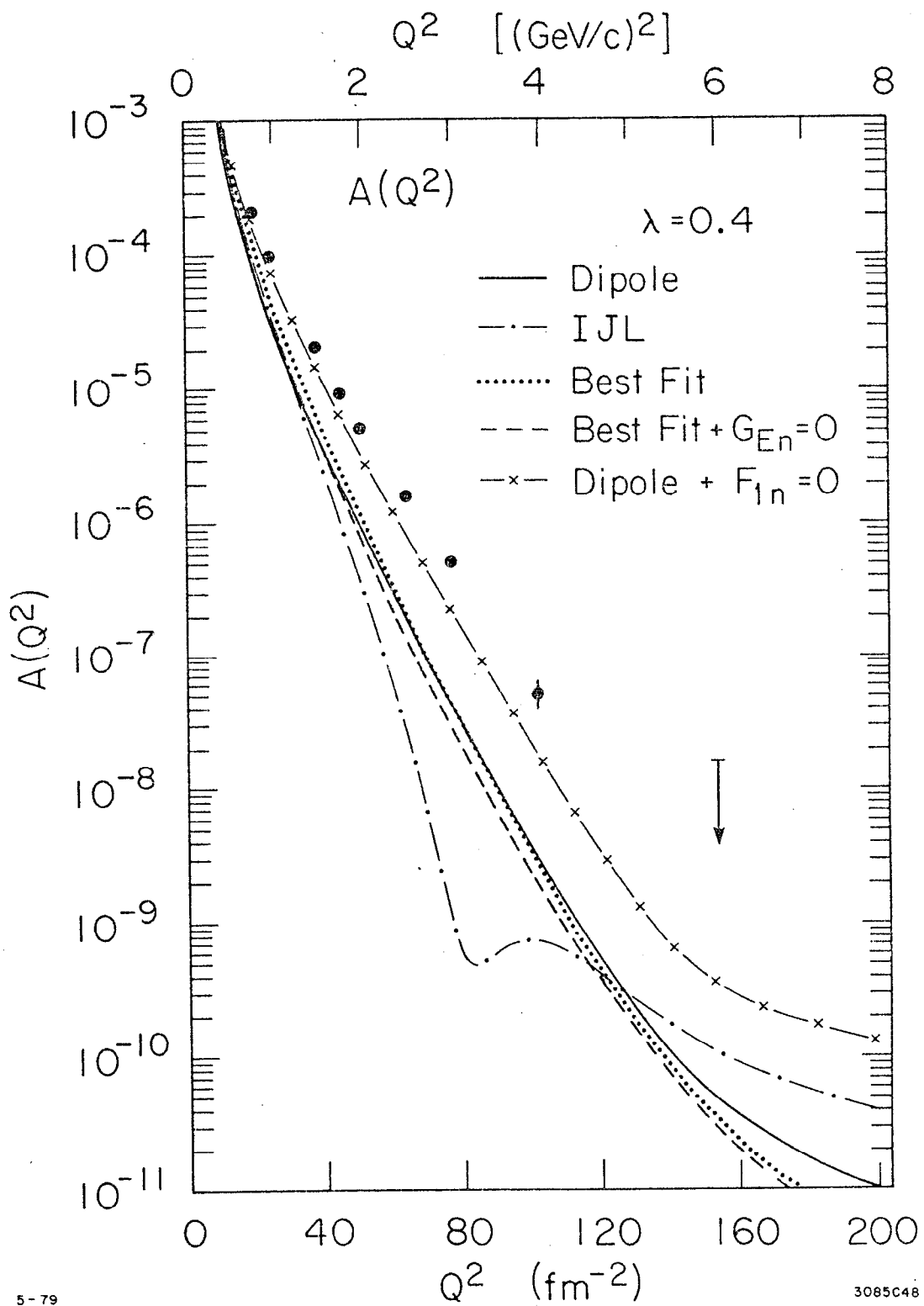


Fig. 19

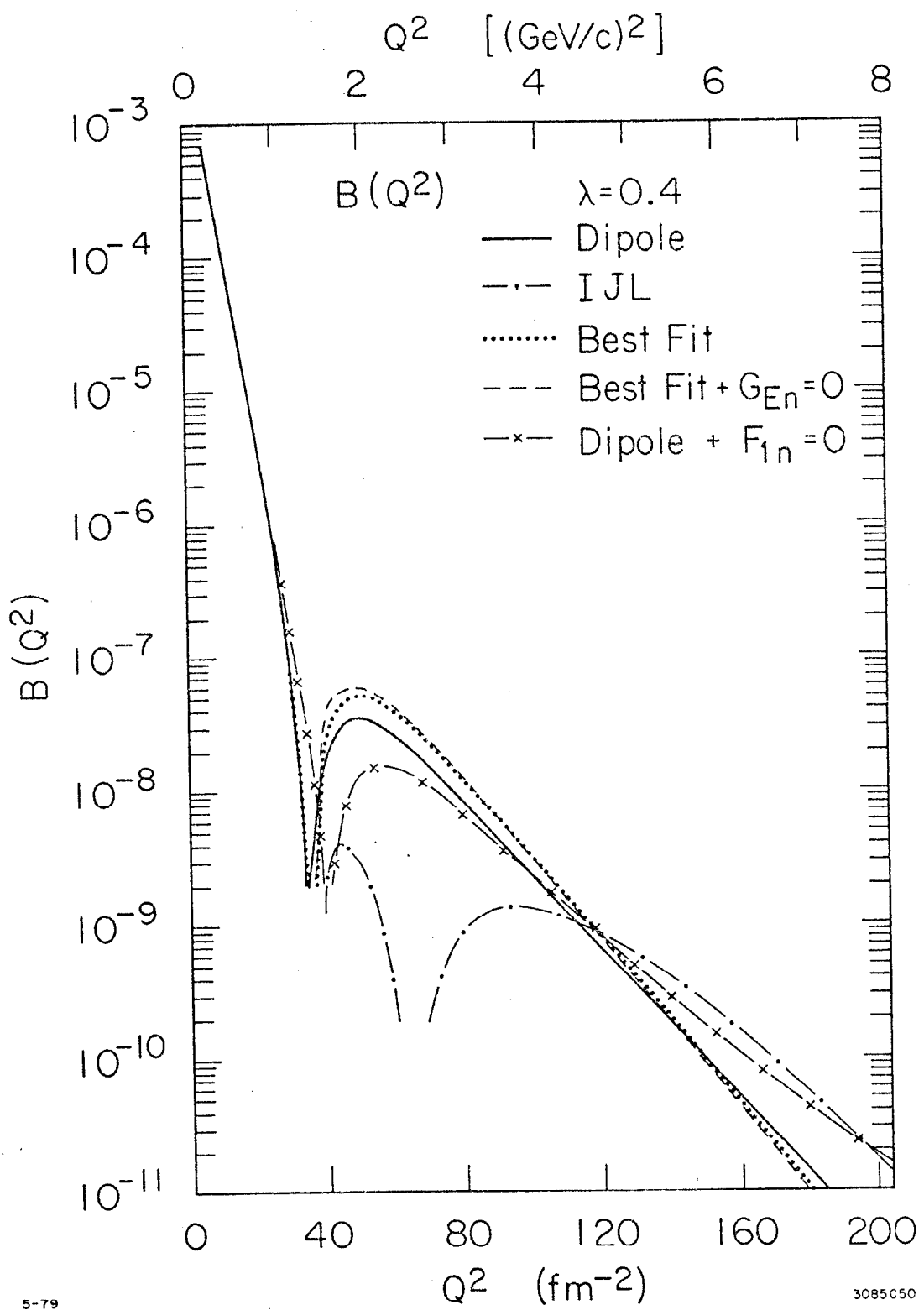
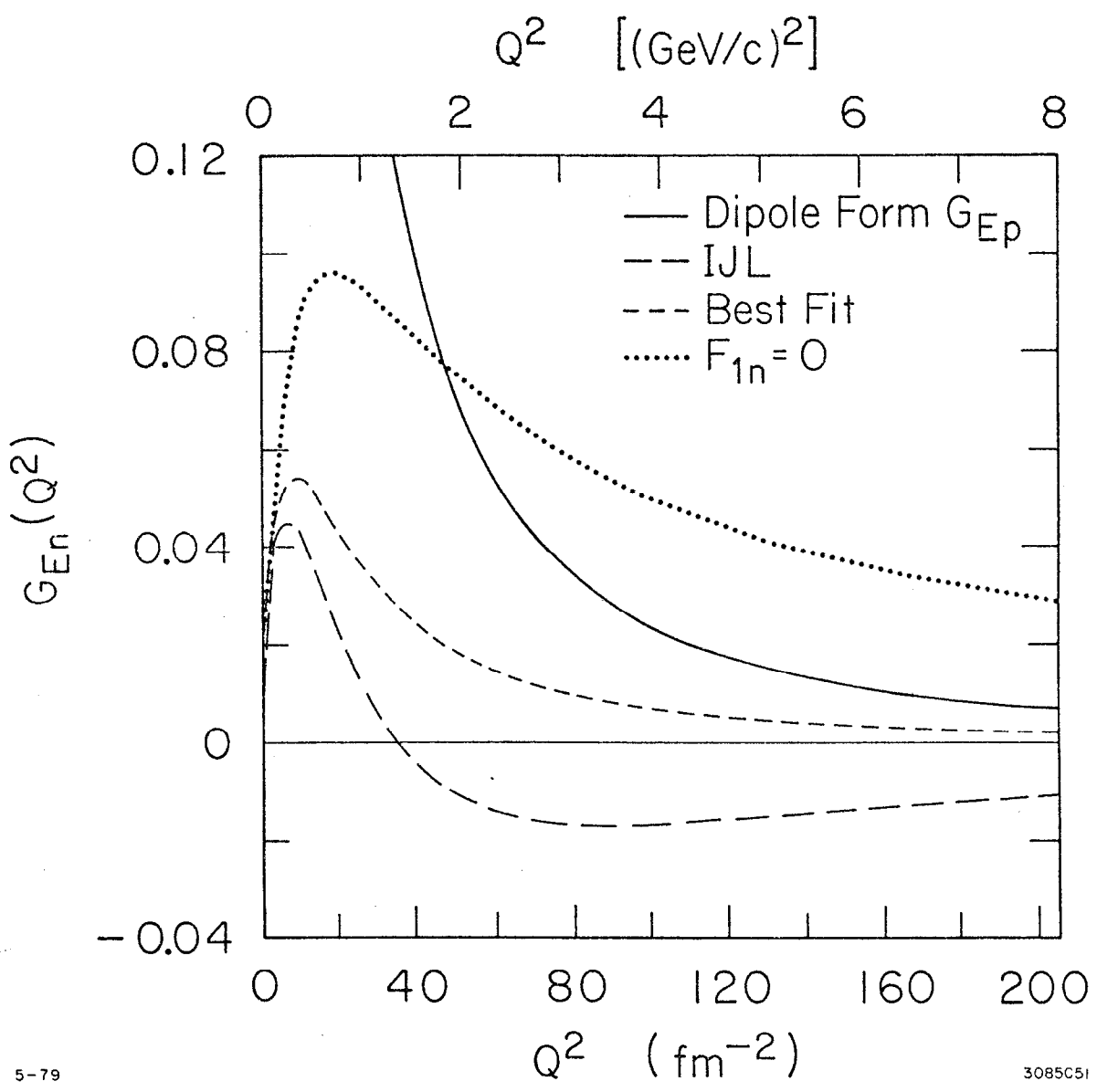


Fig. 20



5-79

3085C51

Fig 21

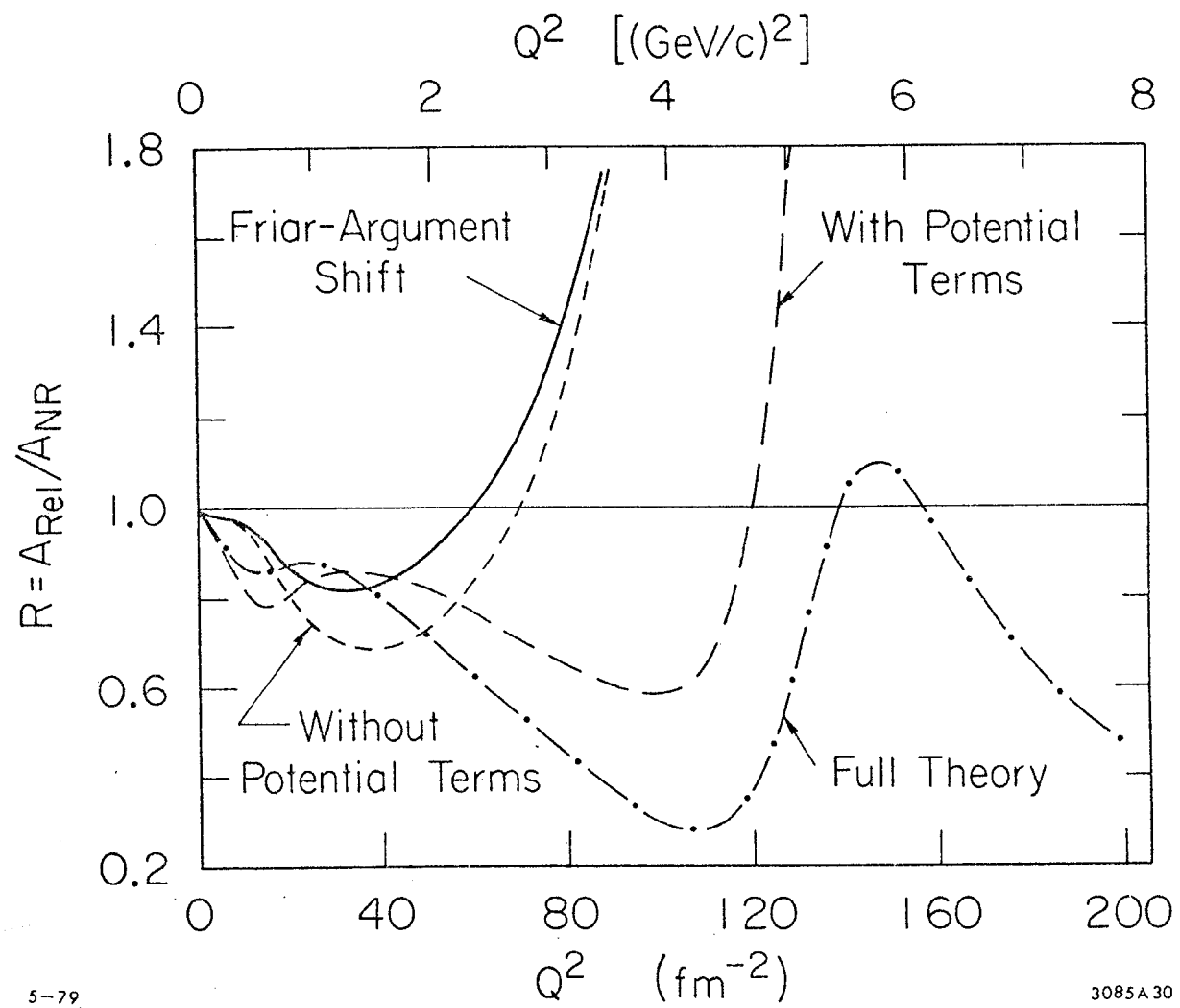


Fig. 22